K-Ar illite and apatite fission track constraints on brittle faulting and the evolution of the northern Norwegian passive margin

Corine Davids[a]*, Klaus Wemmer[b], Horst Zwingmann[c], Fabian Kohlmann[de], Joachim Jacobs[d], Steffen G. Bergh[a]

[a]Department of Geology, University of Tromsø, N-9037 Tromsø, Norway; [b]Geoscience Centre, Georg-August University, 37077 Göttingen, Germany; [c]CSIRO, Earth Science and Resource Engineering, Bentley, WA 6102, Australia; School of Earth and Environment, University of Western Australia, Crawley, WA 6009, Australia; Department of Applied Geology, Curtin University, Perth, WA 6102, Australia; [d]Department of Earth Science, University of Bergen, N-5007, Norway; [e]Neftex, 97 Jubilee Avenue, Milton Park, Abingdon, OX14 4RW, United Kingdom.

E-mail addresses: corine.davids@gmail.com (C. Davids); kwemmer@gwdg.de (K. Wemmer); Horst.Zwingmann@csiro.au (H. Zwingmann); fabiankohlmann@gmail.com (F. Kohlmann); Joachim.Jacobs@geo.uib.no (J. Jacobs); steffen.bergh@uit.no (S.G. Bergh)

* Corresponding author: +47 91858314

Abstract

Determining the timing of post-Caledonian brittle faulting in northern Norway is important for the understanding of the extensional tectonic evolution of the north Norwegian continental margin. Fault gouges from the Troms and Vesterålen regions of northern Norway yield Carboniferous to Permian and Carboniferous to Cretaceous K-Ar illite ages, respectively. The results show a contrast in fault activity and exhumation between the Troms and the Vesterålen regions: while major faulting in the Troms region appears to have ceased after the Permian faulting event, faulting continued into at least the Cretaceous in the Vesterålen region. The findings highlight

the importance of a widespread Permian tectonic event followed by a distinct southwestward migration of post-Permian tectonic activity on the north Norwegian passive margin. Late Triassic to Early Jurassic apatite fission track ages do not show significant age offsets across major fault zones in Troms, indicating that most or all of fault activity took place prior to the Late Triassic. The thermal history models are consistent and indicate continuous cooling to about 60˚C in the Late Permian-Triassic.

Keywords: K-Ar illite dating; AFT thermochronology; northern Norway; brittle faulting; post-Caledonian; North Atlantic margin

Abbreviations

AFT, apatite fission track; MTL, mean track length; PAZ, partial annealing zone; BSFC: Bothnian-Senja Fault Complex; HFFZ: Hadselfjorden Fault Zone; LVA, Lofoten-Vesterålen Archipelago; SB: Store Blåmann; SEF: Stongelandseidet Fault; TFFC, Troms-Finnmark Fault Complex; TT: Tromsdalstinden; VF: Vannareid Fault; VVFC, Vestfjorden-Vanna Fault Complex; WLBFZ, West Lofoten Border Fault Zone; WTBC: West Troms Basement Complex.

1. Introduction

Rapid exhumation and cooling in the late stages of the Caledonian collisional event brought the rocks of northern Norway into upper crustal levels. The more than 300 million years long post-Caledonian extensional history of northern Norway is dominated by brittle faulting due to rifting and passive margin evolution. Geologically old brittle fault zones tend to be the result of multiple reactivation events and have therefore often a complex kinematic and thermal history (e.g. Viola et al., 2009, 2013), making the dating of these fault zones challenging. Erosion and poor exposure of many brittle fault zones, concealed by water and sediments in fjords and river

valleys, further complicate the study of post-Caledonian brittle tectonics. As a result, little information is available on the timing of post-Caledonian brittle faulting and exhumation onshore in northern Norway. Apart from a handful of direct ages on fault activity from paleomagnetic dating by Olesen et al. (1997) and $^{40}Ar/^{39}Ar$ dating of reset K-feldspar by Steltenpohl et al. (2009, 2011) and indirect ages through apatite fission-track (AFT) analysis, with age offset across faults in the Lofoten-Vesterålen archipelago (Hendriks, 2003; Hendriks et al., 2010), all tectonic interpretations are speculative and based on correlation of onshore fault orientations with offshore fault trends and their known timing.

Determining the timing of the brittle fault activity and exhumation in the coastal areas of northern Norway is essential for the understanding of the extensional tectonic history of the North Atlantic margin, and in particular of the relationship between offshore and onshore tectonics. In this paper, we combine new K-Ar illite data from fault gouges with new AFT data from across a number of major fault zones in the Troms and Vesterålen areas in northern Norway to improve our understanding of the timing of brittle faulting and associated exhumation in the Troms and Vesterålen areas.

2. Geological setting

The study area (Fig. 1 and 2) is located on the northern Norwegian continental margin across the transition from the rifted Lofoten-Vesterålen margin to the sheared SW Barents Sea margin (Faleide et al., 1993, 2008; Tsikalas et al., 2012). The Senja Fracture Zone, which formed in the early Tertiary, possibly by reactivation of structures related to the Bothnian-Senja fault complex (Faleide et al., 1993, 2008;

Mosar, 2003; Tsikalas et al., 2012) forms the boundary along the sheared SW Barents Sea margin. The North Atlantic passive margin started to develop following the Caledonian orogenic collapse in the Late Devonian to Carboniferous. Rifting took place during a succession of pronounced rift phases in the Late Permian/Early Triassic, the Mid/Late Triassic, Early Cretaceous, mid Cretaceous, and latest Cretaceous to Paleogene (e.g. Blystad et al., 1995; Brekke, 2000; Doré, 1991; Doré et al., 1999; Lundin and Doré, 1997; Mosar et al., 2003; Ziegler, 1989) and resulted in continental break-up and drifting in the Early Tertiary (e.g. Olesen et al., 2007; Talwani and Eldholm, 1977).

The geology onshore in western Troms and the Lofoten-Vesterålen Archipelago (LVA) is characterised by Precambrian basement provinces in the west (Bergh et al., 2010; Corfu, 2004, 2007; Griffin et al., 1978; Zwaan, 1995), which are separated from the Caledonian nappes in the east by Caledonian ductile thrusts and post-Caledonian brittle faults (Andresen and Forslund, 1987; Olesen et al., 1997). The Precambrian basement provinces are only weakly influenced by Caledonian deformation (e.g. Corfu et al., 2003). The basement rocks form a NE-SW trending horst system, which is bounded by the Vestfjorden-Vanna Fault Complex (VVFC) (Andresen and Forslund, 1987; Olesen et al., 1997) to the east and the Troms-Finnmark Fault Complex (TFFC) (e.g. Gabrielsen et al., 1990; Waqas, 2012) and the West Lofoten Border Fault Zone (WLBFZ) (Blystad et al., 1995; Hansen, 2009; Hansen et al., 2012a) to the west.

Middle Jurassic to Early Cretaceous sedimentary rocks have been found on the island Andøya in a fault bounded basin (Dalland, 1975, 1981) and in the Late Jurassic Sortlandsundet basin in the sound between the islands Hinnøya and Langøya of the LVA (Davidsen et al., 2001; Fürsich and Thomson, 2005).

The offshore geology on the Lofoten-Vesterålen margin is characterised by dominantly N-S to NE-SW trending ridges and basins bounded by normal faults and filled with Mesozoic to Cenozoic sedimentary rocks (Bergh et al., 2007; Blystad et al., 1995; Hansen et al., 1992; Hansen et al., 2012; Tsikalas et al., 2001). The LVA forms part of a ridge with a distinctively thinned continental crust, which has been attributed to the development of a core complex at middle to lower crustal levels during late to post-Caledonian extension (Steltenpohl et al., 2004; Tsikalas et al., 2005). The basin bounding fault zones on the Lofoten-Vesterålen margin continue into the SW Barents Sea margin and link up with the TTFC (e.g. Gabrielsen et al., 1990; Waqas, 2012), which separates the Finnmark platform to the east from a series of basins (Hammerfest basin, Tromsø basin, Harstad basin), which may have been initiated as early as the Carboniferous, to the west (Barrére et al., 2009; Tsikalas et al., 2012).

2.1. Onshore-offshore correlation

Offshore fault systems on the continental shelf in northern Norway are relatively well understood through the study of seismic data and well data (e.g. Hansen, 2009; Hansen et al., 2012; Tsikalas et al., 2001, 2005). The timing of onshore fault systems, however, is more speculative and mostly obtained through correlation of fault orientations between onshore and offshore brittle fault systems (Bergh et al., 2007; Eig et al., 2011; Hansen et al., 2012; Wilson et al., 2006). The two dominant NNE-SSW and ENE-WSW trending fault systems form a rhomboid shaped geometry and Wilson et al. (2006) and Hansen et al. (2012) concluded that these two systems were active simultaneously from the Early Triassic (Hansen et al., 2012) or Late Jurassic (Wilson et al., 2006) to the Early Cretaceous. Bergh et al. (2007) and Eig et al. (2011), however, preferred a tectonic model whereby the NNE-SSW trending fault zones

were formed during a Permian-Jurassic rifting phase, and the ENE-WSW trending fault zones during an Early to Late Cretaceous rifting phase. Hansen et al. (2012) also reported a set of younger NE-SW to E-W trending faults that were formed or reactivated during the Late Cretaceous to the Paleogene. Less dominant NW-SE trending fault zones were interpreted to be either Late Cretaceous-Paleogene strike-slip faults (Bergh et al., 2007; Wilson et al., 2006), neotectonic joints (Hansen and Bergh, 2012) or formed simultaneously with the two dominant fault orientations in the Late Cretaceous (Hansen et al., 2012).

2.2. Previous geochronology

Muscovite $^{40}Ar/^{39}Ar$ ages indicate that the rocks of the Caledonian belt in Troms cooled to below about 425˚C (Harrison et al., 2009) between 427-373 Ma (Anderson et al., 1992; Coker et al., 1995; Dallmeyer and Andresen, 1992). Similar ages have been reported from the Precambrian basement provinces in Troms and the LVA (Dallmeyer, 1992; Hames and Andresen, 1996; Steltenpohl et al., 2004, 2011) suggesting that the whole region had cooled to below about 425˚C by the Middle to Late Devonian.

Brittle faulting may have started as early as the Carboniferous. Corfu et al. (2003) reported U-Pb ages of 350-320 Ma for an unidentified U-rich mineral on Kvaløya and suggested that hydrothermal activity related to brittle faulting may have led to the deposition of these U-rich minerals. Palaeomagnetic dating of two brittle faults in Precambrian basement, thought to be associated with the VVFC, on the islands Kvaløya and Senja identified two phases of fault activity: an early Permian phase overprinted by a Tertiary-recent phase (Olesen et al., 1997, 2002). Olesen et al. (1997) associated the Permian phase with the formation of cataclasite, fluid circulation and

the precipitation of hematite, and the Tertiary-recent phase with the formation of fault gouge. $^{40}Ar/^{39}Ar$ age spectra of hydrothermally altered K-feldspar from brittle fault zones related to the VVFC indicate an Early to Mid Permian phase of fault activity (Steltenpohl et al., 2009; Davids et al., 2010, 2012b, 2012c). In contrast, altered K-feldspars from brittle fault zones in the Vesterålen yielded younger ages and their $^{40}Ar/^{39}Ar$ age spectra were interpreted to indicate a Middle Triassic to Early Jurassic phase of fault activity (Steltenpohl et al., 2011).

Published AFT ages from the Troms region (excluding the LVA) indicate a regional cooling phase in the Late Triassic- Jurassic, with a decrease in ages from about 200 Ma in the north to about 145 Ma in the south (Hendriks, 2003; Hendriks et al., 2007). AFT and (U-Th)/He results from a vertical profile of Tromsdalstinden, a 1234 m high mountain immediately east of the city of Tromsø (Fig. 9), show rapid cooling in the Late Triassic – Early Jurassic followed by lower cooling rates during the Middle Jurassic – Early Cretaceous (Hendriks, 2003). AFT age patterns in the LVA, however, show a clear age jump across the Hadselfjorden fault zone (HFFZ), with 237-144 Ma ages in the hanging wall to the NW and 150-72 Ma ages in the footwall to the SE with tilting to the SE (Hendriks et al., 2010). The age patterns show a km-scale half-dome shaped footwall uplift during the Late Mesozoic, which may have continued or was reactivated in the Cenozoic (Hendriks, 2003; Hendriks et al., 2010).

At a larger scale, the AFT ages in northern Norway show an NE-SW trending oval pattern with the youngest, Late Cretaceous, ages in the centre; the centre is located immediately southeast of the LVA (Hendriks et al., 2007). The AFT ages show a general westward younging with an asymmetric pattern typical for a rift shoulder that has undergone scarp retreat (Hendriks et al., 2007). The current study area (Fig. 2) is

located on the northern flank of the large-scale oval AFT age pattern with ages increasing to the north and east.

3. Methods

3.1. K-Ar illite analysis

Fresh fault gouges samples were collected from quarries and road cuts after removing 5-15 cm of surface material. Sample preparation and analysis of 7 samples was carried out at the University of Göttingen, Germany; for 3 samples (Vannøya faultgouge, Laksvatn faultgouge and Laksvatn slickenslides) the sample preparation and analysis was carried out at CSIRO, Australia. Fault gouge material was mixed with demineralised water and anticoagulent (tetra-sodiumdiphosphate decahydate), sieved at <125 μm, and the size fractions 2-6 μm and <2 μm were separated according to Stoke's Law. The <0.2 and <0.1 μm size fractions were obtained using an ultra-centrifuge. The size fractions were dated using conventional K-Ar geochronology (Dalrymple an Lanphere, 1969). The potassium content was determined in duplicate by flame photometry and the argon isotopic composition was measured using isotope dilution and mass spectrometry according to procedures described by Wemmer (1991) and Löbens et al. (2011) for the analyses carried out in Göttingen, and by Zwingmann et al. (2011) for the analyses carried out at CSIRO. In Göttingen the ^{38}Ar spike used for isotope dilution was calibrated against the biotite standard HD-B1 (Fuhrmann et al., 1987) and at CSIRO against the biotite standard GA 1550 (McDougall and Roksandic, 1974). The age calculations are based on the decay constants recommended by the IUGS (Steiger and Jäger, 1977). The analytical error for the K-Ar results is given at a 95% confidence level (2s).

The mineralogy and illite crystallinity were investigated by XRD analysis on air-dried and glycolated samples. In Göttingen this was carried out using a Philips PW 1800 X-ray diffractometer following the procedures described by Löbens et al. (2011); at CSIRO the samples were analysed with a Philips automated EPD 1700 X-ray diffractometer using CuKα radiation and 40 KV/30 mA, following procedures described by Zwingmann et al. (2011).

The clay mineralogy of selected gouge samples was investigated by scanning electron microscope (SEM, Zeiss Evo). A few small chips of each sample were mounted on a carbon tape and coated with Carbon. A JEOL 2010 TEM (200 kV) was used for detailed, grain-by-grain morphological characterization of selected clay fractions. Samples were prepared by placing one drop of clay solution on a micro carbon grid film and drying in air. The chemical composition of individual particles was investigated by an attached energy dispersive spectrometry (EDS) system.

3.2. Apatite fission track analysis

Apatite separates were obtained using standard mineral separation techniques. Apatite grains >100 μm were mounted in epoxy, cut and polished to expose internal mineral surfaces, and etched in 5 molar HNO_3 for 20 seconds at 20 ± 0.5 °C. Uranium contents were determined using the external detector method (EDM) (e.g. Tagami and O'Sullivan, 2005). The apatite mounts were packaged together with 4 Uranium spiked standard glass dosimeters IRMM-540R (15 ppm U) to monitor the neutron fluence. The packages were irradiated at the FRM II research reactor at the Technical University of München in Germany. After irradiation, the mica detectors were etched in 40% HF at room temperature for ca 18 minutes to reveal the induced tracks. The

zeta calibration method (Hurford and Green, 1983) was used to determine the AFT ages; a personal zeta factor of 261.5 ± 6.1 was established by counting Durango and Fish Canyon standards from 5 different irradiations. Fission tracks were counted at 1250x magnification on an Olympus BX51 optical microscope with an attached drawing tube and a digitising tablet at the University of Bergen, using a computer-controlled stage, driven by the FT-Stage software (Dumitru, 1993). Horizontal confined track lengths, their angle with the crystallographic c-axis and D_{par} were measured at a 2000x magnification. AFT ages were calculated using MacTrack X (Noble, 2002). All obtained AFT ages are quoted as central ages (Galbraith and Laslett, 1993) with 1 standard error uncertainty.

4. Results

4.1. Brittle fault descriptions

Most of the faults sampled in this study are part of a network of faults that form the rhomboid-shaped fault pattern of NNE-SSW and ENE-WSW trending faults that dominate the northern Norwegian Atlantic margin (Fig. 1 and 2). Of the two sets of faults, the (E)NE-(W)SW trending faults are best represented (Fig. 5 and 7). A third set of faults trending (W)NW-(E)SE is only represented by one fault in this study. Apart from the fault near Laksvatn, which is located in the Caledonian nappes, all faults described in this paper are situated in the Precambrian basement (Fig. 2).

Laksvatn (Fig. 2 and 3a): The NE-SW trending brittle fault near the town Laksvatn is located in a unit of fine-grained mica-schist in the upper allochthon of the Caledonian nappes. The mica-schist shows tight to isoclinal folds with subhorizontal fold axes and a dominant flat-lying axial plane cleavage. The ca 50 cm wide fault zone dips 65° to the NW and is composed of strongly fractured rock with a 5-10 cm wide zone with fault gouge below the hanging wall. Slickenside striations indicate a down to the NW movement.

Vanna (Fig. 2 and 3b): This sample was taken from the ENE-WSW trending Vannareid Fault (VF) on the island Vanna, which separates variably deformed tonalitic gneiss in the footwall to the north from mylonitic tonalitic gneiss in the hanging wall (Opheim and Andresen, 1989). The fault zone dips about 50° to the SSE. The fault is only partially exposed, but consists of >5 m wide complex zone with (ultra)cataclasite, fault breccia, fault gouge and abundant quartz and carbonate veins. Moderate to shallow S-plunging slickenside striations indicate oblique normal faulting. However, the zone is complex with at least 2 generations of cataclasite and

fault gouge and has likely experienced multiple periods of faulting. It is uncertain which faulting event is reflected in our K-Ar data.

Sifjord (Fig. 2 and 4a): The ENE-WSW trending fault zone is oriented parallel to the fjord Sifjorden on the west coast of Senja (Gagama et al., 2005). The fault zone dips steeply to the NNW and is located in granitic gneiss. The fault core is exposed in a road cut and consists of a 1.5 m wide zone with strongly fractured rocks, cataclasite and a 2-5 cm wide zone with fault gouge immediately below the hanging wall. Fracture orientations and slickenside striations indicate down to the NNW movement.

Andøya (Fig. 2 and 3c): The N-S trending fault zone in the northeast of the island Andøya is exposed in a quarry. The fault zone dips about 40° to the E. The sample was taken from a 5-10 cm thick layer of fault gouge separating strongly fractured gabbro (biotite-schist) in the footwall from massive migmatitic gneiss with a steep SW-dipping foliation in the hanging wall. Slickenside striations indicate down to the E movement. This fault zone is parallel to the Jurassic-Cretaceous basin to the east (Dalland, 1981).

Rødsand (Fig. 2 and 3d): This sample was taken from the major NE-SW trending Hadselfjorden fault zone (Hendriks et al., 2010; Osmundsen et al., 2010) exposed in a large active quarry at Rødsand on Hinnøya. The main exposed fault plane dips about 40° to the NW and shows down-dip slickenside striations indicating down to the NW movement. The footwall consists of several meters of green cataclasite, while the hanging wall damage zone is characterised by tens of meters of strongly fractured rocks, fault breccia and cataclasite. The sample was taken from a 5 cm thick layer of fault gouge immediately overlying the main fault plane.

Ryggedalsvatn (Fig. 2 and 3e): The NE-SW trending fault zone is located in Precambrian granitic gneiss near Ryggedalsvatn on Langøya. The fault zone dips about 55° to the NW and consists of an up to 2 m wide zone with cataclasite, fault breccia and fault gouge. The fault surface contains moderately W to NW plunging striations, suggesting a down to the NW movement.

Straumsnes (Fig. 2, 4b and 4c)**:** The NNE-SSW trending fault zone, located in Precambrian granitic gneiss, is exposed in two sides of an abandoned quarry near Straumsnes on Langøya. On the northern side (Fig. 4b), the 2 m wide fault zone dips about 65° to the ESE and is composed of fault breccia, highly fractures granite and a 10-20 cm wide zone of fault gouge. Two sets of slickenside striations, one set plunging shallow to the SSW and another set plunging steeply to the ENE, indicate both strike-slip and normal movement. Sample Straumsnes 1 was taken from this fault gouge.

On the southern side (Fig. 4c), two 1 m wide steeply E-ESE-dipping fault zones are separated by about 5 m of massive granitic gneiss. Both zones contain a 20-30 cm wide zone of fault gouge and fault breccia. Striations on the wall rock of the western zone plunge ca 10° to the SSW, while striations on the wall rock adjacent to fault gouge in the eastern zone plunge ca 70° to the SSW. Sample Straumsnes 2 was taken from dark red brown fault gouge in the western zone.

Instøya (Fig. 2 and 3f): This NE-SW trending fault zone on the island Instøya dips ca 70° to the SE and defines the contact between strongly foliated tonalitic gneiss in the south and a more mafic unit in the north. The 5 m wide fault zone is parallel to the gneissic foliation and contains a 50 cm wide zone of unconsolidated fault gouge and fault breccia adjacent to the gneiss. The remaining fault rocks are strongly fractured

fine-grained diorite and a 1-2 m wide fractured pegmatite. Iron oxide coated fracture surfaces in the diorite and pegmatite show shallow WSW-NW plunging striations with a possible sinistral strike-slip sense of movement.

Myre (Fig. 2): The WNW-ESE trending fault zone near the town Myre on Langøya dips moderately to the SSW. The 1-2 m wide strongly fractured zone is located in fine-grained diorite and includes a 1 cm thick fault gouge layer and a 10 cm wide zone with fault breccia. Striations on the fault surfaces plunge shallowly to the SSE and suggest an oblique normal sense of movement.

4.2. K-Ar fault gouge data

The K-Ar results are summarised in Table 1 and in Fig. 6; the locations of the dated faults are mapped in Fig. 2. Uncertainties are quoted at a 2σ level. The different fault gouge samples show a significant variation in the K_2O content, from 0.27 to 6.16 wt% (Table 1). The fault gouges from the faults Myre, Instøya, and Rødsand in the Vesterålen, and from the fault on Vanna in the north of the study area have K_2O contents of less than ca 1.5 wt% in all size fractions. This means that these fault gouges have low concentrations of K-bearing minerals such as illite. The sample from Instøya has also rather low radiogenic ^{40}Ar contents, which resulted in relatively high analytic uncertainties due to error magnification (McDougall and Harrison, 1999), and the results for this fault should be considered with caution.

Three size fractions were analysed from all faults apart from the fault at Laksvatn (Table 1; Fig. 6). For this fault only the <2 μm fraction of the fault gouge was analysed, in combination with a whole rock sample of chlorite slickensides from the

adjacent wall rock. Most of the results show progressively older ages with increasing grain size; however, samples Vanna, Sifjord and Straumsnes 2 show different trends. Straumsnes 2 shows an inverse relationship with increasing K-Ar ages with decreasing grain size, and for samples Vanna and Sifjord the middle size fractions yield the oldest age.

The measured individual K-Ar ages range from 116.2 ± 3.0 Ma to 978.2 ± 9.9 Ma (Table 1; Fig. 6), with the majority of the ages between 116 Ma and 400 Ma. The ages of 521.6 Ma and 978.2 Ma from the fault near Myre are anomalously old and may be contaminated by inherited material from the Precambrian wall rock. The spread in ages of the different size fractions from the same sample vary from ca 30 Ma (Rødsand) to ca 140 Ma (Straumsnes 2).

Plotting the measured ages against the orientation of the faults (Fig. 7) shows that, in this study, the ENE-WSW and N-S trending faults only yielded Carboniferous-Permian K-Ar illite ages. The NNE-SSW and NE-SW trending faults show a much larger age spread from Carboniferous to Cretaceous. The only dated NW-SE trending fault near Myre has a maximum age of ca 300 Ma with the larger size fractions most likely being dominated by inherited material.

4.3. Fault gouge mineralogy and morphology

The mineralogy of the fault gouges is quite variable (Table 2). Only the samples from the faults at Laksvatn and in Sifjord contain considerable amounts of illite. The illite has been identified as high temperature illite $2M_1$, which cannot be distinguished from muscovite by XRD analysis. Most samples are dominated by smectite and chlorite,

with variable amounts of quartz. The coarse 2-6 μm size fractions from the faults at Ryggedalsvatn, near Straumsnes (sample Straumsnes 1) and the fault on Instøya contain minor amounts of feldspar, while four other coarse size fractions (Sifjord 2-6 μm, Straumsnes 1 <2 μm, Straumsnes 2 2-6 μm, Myre 2-6 μm) contain trace amounts of feldspar. Inherited feldspar is derived from the Precambrian host rock and can affect the K-Ar age of the sample. Host rock K-feldspar in the WTBC yield integrated $^{40}Ar/^{39}Ar$ ages of between 325 and 515 Ma (Davids et al., 2012b, 2012c), but no ages are available from host rock K-feldspar in the Vesterålen.

Whole rock fault gouge sample characterisation by SEM of the faults near Laksvatn and on Vanna indicate that the gouges contain authigenic clay minerals comprising illite with plates and fibrous illite/muscovite morphology (Fig.8a). TEM investigations confirmed occurrence of mainly authigenic platy and minor fibrous illite clay minerals in the separated fractions (Fig. 8b). Detrital illite normally shows irregular edges, while authigenic illite particles have sharp and well-defined ideomorphic euhedral edges (Clauer and Chaudhuri, 1995). Illite was confirmed by EDS analyses for SEM and TEM investigations.

4.4. Apatite fission track ages and thermal history modelling results

The samples were collected along two WNW-ESE transects across Troms (at a latitude of approximately N 69.7˚ and N 69.4˚), crossing a number of major NE-SW and ENE-WSW trending fault systems, notably the VVFC (Fig. 9). In addition, 6 samples were collected at 200 m elevation intervals up the 1044 m high mountain Store Blåmann, located 10 km west of Tromsø, with a total horizontal sampling distance of about 1.5 km. The samples along this elevation profile are all of the same

rock type, granite. Unfortunately, several samples taken from the Caledonian nappes contained little or no apatite, leaving a large gap without AFT age information in the northern transect.

Counting details are summarised in Table 3 and AFT ages, with uncertainties quoted at a 1σ level, are plotted on the map in Fig. 9. AFT ages vary from 223 ± 19 Ma to 182 ± 6 Ma (Table 3, Fig. 9). The measured D_{par} range from 1.4 μm to 1.9 μm. Plotting the kinematic annealing parameter D_{par} against AFT age shows that, apart from 2 outliers with high D_{par} values, samples S09/111A and S09/17, all samples plot in a cluster, which indicates that there is no correlation between the measured age and the chemical composition of the apatites (Fig. 10). However, outlier S09/111A contains hydroxyl fluorapatites (Broska et al., unpublished data), and the different chemical composition could explain the higher D_{par} of 1.9 μm. The replacement of F by OH tends to lead to slower annealing rates, which again results in older AFT ages (Donelick et al., 2005). Moreover, apatites from sample S09/111A are characterised by abundant rod-shaped pyrrhotite and other mineral inclusions parallel to the crystallographic c-axis (Broska et al., unpublished data), and the effect of these inclusions on the annealing rate or on the fission track counts is unknown. Although only grains that appeared to be inclusion free were chosen for AFT analysis, the abundance of inclusion rich grains in this sample means that also the apparently inclusion free grains could be affected by some of these effects.

The only possible AFT age offset across faults in the study region can be seen in the age profile of the northern transect (Fig. 11). Here, the difference in AFT ages of 186 ± 7 Ma (sample S09/102) to the west and 223 ± 19 Ma (sample S09/111A) to the east of the major fault zone that forms the boundary between the Caledonian nappes and

the Precambrian basement (Fig. 9) could be interpreted as indicating Jurassic or more recent faulting along this fault zone. However, sample S09/111A, as described above, has a different chemistry and unusual inclusions that could affect the annealing rate. Furthermore, this sample lies in the same block as sample S10/14 with an age of 186 ± 9 Ma. Without more data, we are therefore reluctant to conclude that there is an age offset across this fault based on the AFT age of one, somewhat unusual, sample. We prefer to interpret that the new AFT data show neither systematic WNW-ESE age trends nor any significant age differences across major faults.

The AFT ages along the age-elevation profile of the Store Blåmann mountain vary between 204 ± 8 Ma and 186 ± 8 Ma and apart from one outlier at an elevation of 608 m and an age of 204 ± 8 Ma, all samples are within one standard deviation of the mean. The age-elevation profile shows no significant increase in AFT ages with increasing elevation (Fig. 12). In contrast, the bottom half of the age-elevation profile shows a slight inverse trend with the oldest AFT age at the lowest elevation. The AFT ages along the profile and the lack of an age trend are consistent with results from a vertical profile of the Tromsdalstind mountain in the Caledonian nappes reported by Hendriks (2003); this age-elevation profile is located about 15 km east of the Store Blåmann across a major fault zone (Fig. 9). Both profiles suggest rapid cooling through the partial annealing zone, although the slight inverse trend could also indicate offset across minor unknown faults.

Four samples along the northern profile and one from the island of Senja yielded enough horizontal confined fission tracks to run inverse thermal history models. HeFTy 1.6.7 (Ketcham, 2005) was applied for inverse thermal history modelling using the annealing model of Ketcham et al. (2007), with D_{par} as a kinetic annealing parameter, and the c-axis projection model by Ketcham et al. (2007). Timing

constraints used for the modelling are shown as boxes in Fig. 13. The initial constraint box is based on the ages of the faults in Sifjord and on Vanna in the study area. Their ages are presented in this paper, and used with large uncertainties in both age and temperature to avoid restricting the thermal history modelling too much.

The Mean Track Lengths (MTLs) of these five samples vary from 12.85 ± 1.03 μm to 13.83 ± 0.93 μm (Table 3). Three of the four models along the northern profile suggest a cooling rate of 1-2˚C/Ma from 120˚C to 60˚C in the Late Permian – Early Triassic, followed by a long period of slow cooling (<0.2˚C/Ma) from the Triassic to the end of the Cretaceous. Sample S09/116 from the eastern side of the Lyngen peninsula, suggests a slightly later fast cooling in the Triassic rather than the Permian. This sample also contains the longest MTLs, 13.83 ± 0.93 μm, which indicates that less time is spent in the partial annealing zone (PAZ) (Gallagher, 1995). This is reflected in the lower model temperatures in the last 200 Ma than the other models. The fifth model, from sample S09/17 from the island Senja suggests fast cooling in the Late Permian – Early Triassic, similar to the first three models.

Several of the thermal history models show that cooling histories whereby the rocks were exhumed to the surface in the Triassic-Jurassic followed by reburial in the Jurassic-Cretaceous also fit the data well. However, this falls outside the sensitivity range of the AFT analysis. AFT analysis is only sensitive in the temperature range of the partial annealing zone, between about 120-60˚C (Gallagher, 1995). With the current data it is not possible to distinguish between cooling histories exhibiting slow cooling from the Triassic to the Paleogene or cooling histories that include exhumation and reburial, nor is it possible to determine the timing of final cooling and exhumation.

5. Discussion

The results are used to determine the timing of the onshore fault activity and associated exhumation in northern Norway and to highlight the differences between the Troms and the Vesterålen regions. In this section we will first discuss the interpretation of the K-Ar illite results and their implications for the timing of fault activity. This is followed by a discussion of the AFT results and the exhumation history. Finally we will discuss the implications of the new data for the tectonic evolution of the northern Norwegian passive margin.

5.1. Interpretation of K-Ar illite ages

The interpretation of K-Ar illite ages and their general increase in age with increasing grain size is still being debated (e.g. Haines and van der Pluijm, 2008; van der Pluijm et al., 2001; Zwingmann et al., 2010, 2011; Zwingmann and Mancktelow, 2004) and there are a number of different interpretations: 1. Fault gouges are a mixture of crushed inherited material and newly formed clay minerals, whereby the larger size fractions contain more inherited material and less newly formed minerals than the smaller size fractions (e.g. Solum et al., 2005). In this case, all size fractions are mixtures of inherited material and newly formed clay minerals and the youngest age of the smallest size fraction is the least contaminated age, and therefore the maximum age for the fault event. 2. Clay minerals that formed in early stages of faulting have had more time to grow than those formed during later stages of faulting and are therefore larger and older. In this case, the fault gouges are a mixture of clay minerals

formed at different times during faulting (e.g., Zwingmann et al., 2010) and the ages define a minimum age range for the fault activity. 3. Larger grains are more retentive (larger diffusion domain) than smaller grains (e.g. Zwingmann and Mancktelow, 2004). In this case, the youngest age may have been affected by $^{40}Ar^*$ loss and is therefore a minimum age. An inverse age-grain size relationship is sometimes contributed to Oswald ripening, progressive recrystallisation of older larger grains that leads to a partial loss of radiogenic $^{40}Ar^*$ in the larger grains sizes (Eberl and Srodon, 1988).

Host rock contamination is often studied using the Illite Age Analysis approach (Hunziker et al., 1986; Pevear, 1999) where the influence of an inherited component is assessed by measuring the relative contributions of an assumed inherited $2M_1$ polytype (Haines and van der Pluijm, 2008; Solum et al., 2005) and an authigenic $1M_d$ polytype. However, this approach often fails with older fault gouge samples (e.g. Viola et al., 2013) and also fails in this study as the fault gouges contain either $2M_1$ illite or smectite, but no $1M_d$ illite (Table 2). However, as muscovite ages in the area are >380 Ma (Dallmeyer, 1992; Dallmeyer and Andresen, 1992; Hames and Andresen, 1996; Steltenpohl et al., 2004, 2011) and as high-temperature $2M_1$ illite cannot be distinguished from muscovite by XRD-analysis, we interpret the $2M_1$ illite as either authigenic high temperature illite or inherited material that is partially or fully reset during faulting (e.g. Zwingmann et al., 2010).

5.2. Timing of brittle faulting

The oldest fault gouge ages of ca 370 Ma were found in the fault at Laksvatn in the Caledonian nappes (Fig. 2). The two ages, from the <2 μm size fraction of the fault

gouge and from a slickenside whole rock sample, are within 2σ uncertainty of each other. The fault gouge contains a mixture of high temperature $2M_1$ illite, smectite-vermiculite, and chlorite. Muscovite $^{40}Ar/^{39}Ar$ ages in the vicinity of this fault range from 427-422 Ma, recording late Caledonian cooling (Dallmeyer and Andresen, 1992), and are thus significantly older than the illite in the fault gouge. This suggests that the illite is either inherited material that is partially or fully reset during the faulting or newly grown illite formed during brittle faulting at relatively high temperatures, but below the closure temperature of muscovite. Zwingmann et al. (2010) discussed a similar case in their study of Neogene faults in the Swiss Alps and concluded that the high temperature illite had grown during faulting in the anchizone (>280˚C), just below the ductile-brittle transition. For the fault at Laksvatn this interpretation would make the Devonian age of ca 370 Ma a maximum age for the initiation of fault activity. The presence of smectite-vermiculite in the fault gouge, however, indicates that faulting may have continued or that the fault was reactivated later at lower temperatures.

Similarly, the fault in the northeastern part of Andøya gave Late Devonian to Early Carboniferous ages with a relatively tight clustering of ages between the different size fractions, suggesting that this fault was also initiated in the Carboniferous. However, the presence of Middle Jurassic to Early Cretaceous sedimentary rocks in a fault bounded basin (Dalland, 1975, 1981) not far to the east of this fault suggests that there must have been significant (post) Cretaceous vertical offset along faults in this area. The analysed fault is located within Precambrian gneisses and, although it is probably part of the main basin bounding fault zone, there is no evidence of more recent reactivation along this particular fault. Jurassic to Cretaceous reactivation must have taken place along faults that are not currently exposed within the fault zone. However,

the presence of both trace amounts of illite and a major component of illite/smectite (I/S) mixed layered minerals could indicate that initial faulting in the Carboniferous at higher temperatures was overprinted by a later faulting event at a lower temperature.

The faults on Vanna, in Sifjord, on Instøya and the fault near Myre all yielded Carboniferous to Permian K-Ar age ranges. The Myre sample yielded abnormally old ages of >500 Ma for the two larger size fractions, which suggests that the ages are strongly influenced by inherited material from the Precambrian wall rock. As it is uncertain to what extent the smallest size fraction is contaminated with inherited material, the late Carboniferous age can only be interpreted as a maximum age for this fault. The fault gouge samples from Vanna and from Sifjord gave very similar results. In both cases, both the <0.2 (0.1) μm and the 2-6 μm size fractions gave Early Permian ages, while the <2 μm size fractions yielded Carboniferous ages. It is uncertain why the <2 μm fractions are older than the 2-6 μm fractions; one possible explanation could be that the 2-6 μm fractions are contaminated with young I/S, possibly as clusters of small grains. In both samples, the 2-6 μm fractions contain less illite than the <2 μm and in the fault gouge from Sifjord the 2-6 μm fraction also contains more I/S than the <2 μm fraction, which is unusual. The fault gouge from Vanna contains significantly less illite and mostly smectite-vermiculite (Table 2), which is reflected in the low K_2O content (Table 1). The illite is of polytype $2M_1$, but as muscovite ages from Vanna are >400 Ma (Davids et al., 2012a), the illite in the fault gouge is either inherited material that is reset during faulting or newly grown high temperature illite. The fault gouge from Sifjord has a high K_2O content and illite has an illite crystallinity of upper diagenesis (<0.2 μm) to lowermost anchizone (2-6 μm), indicating a temperature of 200°C-250°C (Frey, 1987). The results suggest that both the faults on Vanna and in Sifjord were active during the Early Permian. The

older ages of the higher temperature illite in the <2 μm fracture could indicate that the faults were initiated as early as the Carboniferous. Both these faults are associated with the VVFC, which was analysed by paleomagnetic dating by Olesen et al. (1997). One of the two dated faults in their paper is from the same brittle fault zone as the fault gouge sample from Sifjord. Olesen et al. (1997) interpreted their data to indicate an Early Permian phase of faulting overprinted by a Tertiary-recent phase. The latter phase was thought to be associated with the formation of fault gouge. Our K-Ar age results indicate an Early Permian phase of faulting, and show no indication of a more recent reactivation.

The fault on Instøya has the same Carboniferous to Permian age range and a tentative interpretation is that this fault was active in the Permian. However, the K_2O content is low in all size fractions (0.27 to 0.71 wt%), due to the low illite component in the I/S mixed layered minerals, and the measured $^{40}Ar^*$ is also lower than in other samples (17.7 to 47.6%).

The fault at Ryggedalsvatn yielded Triassic ages with an age spread of 40 million years between the different size fractions. Both the K_2O content and the ages increase with increasing grain size. Muscovite ages elsewhere in the Vesterålen are >400 Ma (Steltenpohl et al., 2011). Our interpretation is therefore that this fault was active during the Late Triassic, possibly with an earlier phase in the Late Permian-Early Triassic.

Two fault gouges yielded Cretaceous ages, the faults at Rødsand and Straumsnes. The fault gouge from the Hadselfjorden fault zone at Rødsand (Hendriks et al., 2010; Osmundsen et al., 2010) gave Late Jurassic to Early Cretaceous ages with an age spread of less than 30 Ma, suggesting that the fault was active in the Cretaceous, but

that some illite and I/S may have formed as early as the Jurassic. This is consistent with the presence of Jurassic sedimentary rocks in the Sortlandsund (Davidsen et al., 2001), the fjord to the northeast of the fault zone, and with the interpretation of AFT ages, which show an age jump from Triassic-Jurassic ages to Early to Late Cretaceous ages across the Hadselfjorden fault zone (Hendriks et al., 2010). Steltenpohl et al. (2011) analysed red coloured K-feldspar from the Hadselfjorden fault zone at Rødsand. The $^{40}Ar/^{39}Ar$ age spectrum showed apparent ages between 207-239 Ma, which were interpreted to indicate the initiation of the Hadselfjorden fault zone in the Late Triassic. Combining these different results suggests initiation of the Hadselfjorden fault zone in the Late Triassic with cataclasis and hydrothermal alteration of the granite, with continuation or reactivation in the Cretaceous at lower temperatures associated with the formation of fault gouge.

Two different fault gouges were analysed from the fault near Straumsnes, with very different results. Straumsnes 1 gave ages ranging from Middle Triassic to Early Cretaceous with a normal age-grain size relationship, while Straumsnes 2 yielded ages ranging from Middle Devonian to Late Permian with an inverse age-grain size relationship. The 2-6 μm fractions yielded similar ages (240.5 Ma and 254.3 Ma). The Middle Devonian ages appear too old but there is no evidence for the presence of contaminating inherited material in the XRD results. Alternatively, the results could indicate an early faulting phase in the Late Permian-Early Triassic with reactivation in the Early Cretaceous. The observation of at least two sets of slickensides indicating both strike-slip and normal movements in this fault zone confirms that the fault has been reactivated.

5.3. Timing of exhumation

The AFT results are consistent with the results of the fault gouge dating. AFT modelling indicates a period of cooling and exhumation in the Late Permian to Late Triassic, which is simultaneous to or immediately following the Permian faulting in northern Norway as demonstrated in the previous section.

In contrast to the LVA, where it has been shown from both AFT data (Hendriks et al., 2010) and from K-Ar dating of fault gouges (this paper) that faulting continued at least until in the Late Cretaceous, faulting in western Troms appears to have mostly ceased after the Triassic. Although minor offsets and reactivation cannot be resolved within the resolution of the AFT method and faulting at low temperatures may not lead to the formation of illite or I/S minerals that can be measured by the K-Ar method, there is currently no evidence of more recent major faulting events in the Troms region.

The AFT modelling results indicate that the region cooled to around or below 60˚C by the Late Triassic – Early Jurassic, which at a geotherm of 20-30˚C/km corresponds to a depth of 2-3 km. The AFT thermal history models cannot distinguish between a geological history of exhumation in the Triassic-Jurassic followed by reburial by Jurassic-Cretaceous sedimentation and renewed exhumation, or a history whereby the area remained more or less stable at a depth of 2-3 km for most of the Jurassic and Cretaceous. However, the U-Th/He data from a vertical profile of Tromsdalstinden, which showed steadily increasing ages from ca 100 Ma at sea level to ca 200 Ma at the top at 1200 m (Hendriks, 2003), support a history of very slow cooling for at least the Jurassic and Early Cretaceous. As there is also no evidence that this region was ever covered by Jurassic-Cretaceous sediments, a history of Permian-Triassic faulting

and exhumation followed by a long period of very slow cooling at depths of 2-3 km is our preferred interpretation.

5.4. Implications for margin evolution

The timing of offshore faulting on the north Norwegian continental margin is well understood from seismic interpretations (e.g. Blystad et al. 1995; Brekke et al. 2000; Faleide et al. 2008; Gabrielsen et al. 1990). On the Lofoten-Vesterålen margin, rifting took place during events in the Late Permian/Early Triassic, the Mid/Late Triassic, Early Cretaceous, mid Cretaceous, and latest Cretaceous to Paleogene (e.g. Blystad et al., 1995; Brekke, 2000; Doré, 1991; Doré et al., 1999; Hansen et al., 2012; Lundin & Doré, 1997; Mosar et al., 2003; Osmundsen et al., 2002; Ziegler, 1989). The main rhomboid fault pattern with NNE-SSW and NE-SW trending faults was likely developed during the Late Jurassic and Early Cretaceous phase. On the SW Barents Sea margin, the Troms-Finnmark fault complex and related faults and major basins started to develop in the Carboniferous (Nordkapp and Tromsø basin). Fault activity continued in the Jurassic-Cretaceous, when significant crustal extension led to the formation of the Harstad, Tromsø, Bjørnøya and Sørvestnaget basins (Faleide et al., 2008; Gabrielsen et al., 1990; Knudsen & Larsen 1997), and into the Eocene with transform movement along the Senja Fracture Zone and the development of the SW Barents Sea margin (Faleide et al. 1993, 2008; Gabrielsen et al. 1990).

The new onshore fault gouge dating suggests that several N-S to NNE-SSW trending faults and ENE-WSW trending faults in the Vesterålen and Troms regions were already active in the Permian and may have been initiated as early as the Carboniferous. This supports interpretations by Hansen et al. (2012) and Wilson et al.

(2006) that these two dominant fault systems were active simultaneously, although it has been shown here that they were active already in the Permian, earlier than in the Triassic as suggested by Hansen et al. (2012). Subsequently, both NNE-SSW and NE-SW trending fault systems were active in the Triassic to the Cretaceous. Triassic and Cretaceous fault ages were only found in the Vesterålen, and confined to NNE-SSW and NE-SW trending faults. From the data in this paper it thus appears that major faulting on the north Norwegian mainland was restricted to the Permian, while faulting continued into the Triassic and Cretaceous further south and west in the Lofoten-Vesterålen archipelago. The data shows that care should be taken when interpreting different fault orientations as separate events. Many studies have demonstrated that strain is often accommodated preferentially along existing weak zones even though they may be oblique to the current stress regime (e.g. Schlische et al., 2002; Holdsworth 2004), resulting in complicated reactivation histories.

One of the main conclusions that can be drawn from the current data is that the initial Permian faulting was widespread and formed both the faults of the Vestfjorden-Vanna fault complex in the east as well as faults further west, such as the Troms-Finnmark fault complex and related faults in the Vesterålen region. After Permian faulting the location of extensional faulting appears to have migrated southwestwards. This largely corresponds with the timing of initial (pre-) and syn-rift tectonic activity on the SW Barents Sea margin that led to the formation of the Nordkapp and Tromsø basins offshore (e.g. Faleide et al. 2008). Most or all of the post Permian extensional deformation in northern Norway must have occurred either offshore west of the Troms region, e.g. along the Troms-Finnmark fault complex, or further southwest on the Lofoten-Vesterålen basement horst. It appears therefore that the main boundary fault (cf. innermost boundary fault (Mosar et al., 2002)), separating areas of active

thinning and extension from more stable continental crust, must therefore have migrated from a location east of the Laksvatn fault to a location further west after the Permian.

The coastal part of the Lofoten and western Troms margin was uplifted in the Late-Cenozoic (Corner 2005) but the timing of final uplift and exhumation is still much debated (Gabrielsen et al., 2010; Hendriks et al., 2010; Lidmar-Bergström et al., 2000, 2007; Mosar et al., 2002; Nielsen et al., 2009, 2010; Olesen et al., 1997; Osmundsen et al., 2007; Redfield and Osmundsen, 2013; Riis, 1996). The results obtained in this study cannot resolve this issue either as the region cools to below the temperature range of the AFT method prior to the final exhumation in the Cenozoic. The Late Triassic-Early Jurassic AFT ages both at sea level as well as from mountain peaks at 1000-1200 m (this study; Hendriks, 2003) indicate that the region was still buried at depths of 2-3 km 180-200 million years ago. U-Th/He ages of about 100 Ma at sea level to about 200 Ma at 1200 m elevation (Hendriks, 2003) suggest slow cooling and about 1 km of exhumation in the Jurassic and Cretaceous.

6. Conclusions

1. The newly obtained K-Ar illite data indicate that onshore brittle faulting may have initiated as early as in the Carboniferous with faulting along both N-S and NE-SW trending faults on Andøya and near Laksvatn. This is simultaneous with the initiation of the Tromsø-Finnmark fault complex.

2. Permian ages for the fault gouges from Sifjord and Vanna are consistent with earlier paleomagnetic dating results reported by Olesen et al. (2002). We interpret that

the Permian ages indicate widespread Permian activity along faults associated with the Vestfjorden-Vanna fault complex.

3. Inverse thermal history modelling of the AFT data indicates that the Troms region cooled from about 120˚C to about 60˚C in the Late Permian – Early Triassic, at a cooling rate of 1-2˚C/Ma. The cooling could be the result of exhumation associated with normal faulting in the Permian.

4. There is no evidence from either AFT thermochronology or K-Ar illite dating that supports post-Permian reactivation of faults in the Troms region.

5. In contrast, K-Ar illite data indicate that faulting continued in the Triassic and middle Cretaceous in the Vesterålen region. This supports previous conclusions from AFT and $^{40}Ar/^{39}Ar$ K-feldspar data that in the LVA major faulting continued in the Triassic and Cretaceous (Hendriks et al., 2010, Steltenpohl et al., 2011).

6. Although brittle faulting mostly ceased after the Permian fault event in the Troms region, faulting continued in the Vesterålen region. Most or all of the post Permian extensional deformation in northern Norway must have occurred either offshore west of the Troms region or further southwest on the Lofoten-Vesterålen basement horst.

Acknowledgements

We acknowledge financial support from Det Norske and Statoil. We thank Anna Ksienzyk for analytical assistance with AFT analysis and discussions, and John-Are Hansen for sampling suggestions and general discussion. Andrew Todd and Mark Raven, CSIRO, are thanked for technical assistance. Horst Zwingmann acknowledges the use of equipment, scientific and technical assistance of the Curtin University

Electron Microscope Facility, which is partially funded by the University, State and Commonwealth Governments. We thank an anonymous reviewer for a detailed and constructive review.

References

Anderson, M.W., Barker, A.J., Bennett, D.G., Dallmeyer, R.D., 1992. A tectonic model for Scandian terrane accretion in the northern Scandinavian Caledonides. Journal of the Geological Society 149, 727-141.

Andresen, A., Forslund, T., 1987. Post-Caledonian brittle faults in Troms: geometry, age and tectonic significance. The Caledonian and Related Geology of Scandinavia conference, Cardiff, 22-23 September.

Barrère, C., Ebbing, J., Gernigon, L., 2009. Offshore prolongation of Caledonian structures and basement characterisation in the western Barents Sea from geophysical modeling. Tectonophysics 470, 71–88.

Bergh, S. G., Eig, K., Kløvjan, O. S., Henningsen, T., Olesen, O., Hansen, J.-A., 2007. The Lofoten-Vesterålen continental margin: a multiphase Mesozoic-Palaeogene rifted shelf as shown by offshore-onshore brittle fault-fracture analysis. Norwegian Journal of Geology 87, 29-58.

Bergh, S.G., Kullerud, K., Armitage, P.E.B., Zwaan, K.B., Corfu, F., Ravna, E.J.K., Myhre, P.I., 2010. Neoarchaean to Svecofennian tectono-magmatic evolution of the West Troms Basement Complex, North Norway. Norwegian Journal of Geology 90, 21-48.

Blystad, P., Brekke, H., Færseth, R. B., Larsen, B. T., Skogseid, J., Tørudbakken, B., 1995. Structural elements of the Norwegian continental shelf. Part II: The Norwegian Sea Region. Norwegian Petroleum Directorate Bulletin 8, 1-45.

Brekke, H., 2000. The tectonic evolution of the Norwegian Sea continental margin with emphasis on the Vøring and More basins. In: Nøttvedt, A. (Ed.), Dynamics of the Norwegian Margin. Geological Society of London Special Publication 167, 327-

378.

Clauer, N., Chaudhuri, S., 1995. Clays and Crustal Cycles. Springer-Verlag, Heidelberg-New York.

Coker, J.E., Steltenpohl, M.G., Andresen, A., Kunk, M.J., 1995. An 40Ar/39Ar thermochronology of the Ofoten-Troms region: Implications for terrane amalgamation and extensional collapse of the northern Scandinavian Caledonides. Tectonics 14, 435-447.

Corfu, F., 2004. U-Pb Age, Setting and Tectonic Significance of the Anorthosity-Mangerite-Charnockite-Granite Suite, Lofoten-Vesterålen, Norway. Journal of Petrology 45, 1799-1819.

Corfu, F., 2007. Multistage metamorphic evolution and nature of the amphibolite-granulite facies transition in Lofoten-Vesterålen, Norway, revealed by U-Pb in accessory minerals. Chemical Geology 241, 108-128.

Corfu, F., Armitage, P.E.B., Kullerud, K., Bergh, S.G., 2003. Preliminary U-Pb geochronology in the West Troms Basement Complex, North Norway: Archaean and Palaeoproterozoic events and younger overprints. Norges geologiske undersøkelse Bulletin 441, 61–72.

Corner, G.D., 2005. Atlantic coast and fjords. In: Seppälä, M. (Ed.), The physical Geography of Fennoscandia. Oxford Regional Environments Series, Oxford University Press, 203-228.

Dalrymple, G.B., Lanphere, M.A., 1969. Potassium-Argon Dating: Principles, Techniques and Applications to Geochronology, 258 pp., W.H. Freeman, San Francisco, California.

Dalland, A., 1975. The Mesozoic rocks of Andøya, northern Norway. Norges

Geologiske Undersøkelse 316, 271-287.

Dalland, A., 1981. Mesozoic sedimentary succession at Andøya, Northern Norway, and relation to structural development of the North Atlantic area. In: Kerr, J.W., Fergusson, A.J. (Eds.), Geology of the North Atlantic borderlands. Canadian Society of Petroleum Geologist Memoir 7, 563-584.

Dallmeyer, R.D., 1992. $^{40}Ar/^{39}Ar$ mineral ages within the Western Gneiss Terrane, Troms, Norway: evidence for polyphase Proterozoic tectonothermal activity (Svecokarilian and Sveconorwegian). Precambrian Research 57, 195-206.

Dallmeyer, R.D., Andresen, A., 1992. Polyphase tectonothermal evolution of exotic Caledonian nappes in Troms, Norway: Evidence from $^{40}Ar/^{39}Ar$ mineral ages. Lithos 29, 19-42.

Davids, C., Benowitz, J.A., Layer, P., 2012a. Constraining the Caledonian tectonic overprint in a Precambrian gneiss terrane in northern Norway. Thermo 2012, 13th International Conference on Thermochronology, Guilin, China, 24-28 August 2012.

Davids, C., Benowitz, J.A., Layer, P., Wemmer, K., Zwingmann, H., Bergh, S.G., 2012b. $^{40}Ar/^{39}Ar$ dating of hydrothermally altered K-feldspar – Permian brittle faulting in northern Norway. Thermo 2012, 13th International Conference on Thermochronology, Guilin, China, 24-28 August 2012.

Davids, C., Bergh, S.G., Wemmer, K., Layer, P., 2010. K-Ar and $^{40}Ar/^{39}Ar$ dating of post-Caledonian brittle faults in northern Norway. Thermo 2010, 12th International Conference on Thermochronology, Glasgow, UK, 16-20 August 2010.

Davids, C., Kohlmann, F., Hansen, J.-A., Benowitz, J.A., Layer, P., Jacobs, J., 2012c. Post-Caledonian onshore exhumation history of Troms, northern Norway, as constrained by K-feldspar $^{40}Ar/^{39}Ar$ and apatite fission track thermochronology.

Norsk Geologisk Forening Onshore-Offshore relationships on the North Atlantic Margin, Trondheim, 17-18 October 2012.

Davidsen, B., Sommaruga, A., Bøe, R., 2001. Final report: Sedimentation, tectonics and uplift in Vesterålen. Phase 1 - Localizing near-shore faults and Mesozoic sediment basins. NGU Report 2001.111, pp 16.

Donelick, R.A., O'Sullivan, P.B., Ketcham, R.A., 2005. Apatite Fission-Track Analysis. In: Reiners, P.W., Ehlers, T.A. (Eds.), Low-temperature thermochronology: techniques, interpretations, and applications. Reviews in Mineralogy & Geochemistry 58, 49-94.

Doré, A.G. 1991. The structural foundation and evolution of Mesozoic seaways between Europe and the Arctic. Palaeogeography, Palaeoclimatology, Palaeoecology 87(1- 4), 441-492.

Doré, A.G., Lundin, E.R., Jensen, L.N., Birkeland, O., Eliassen, P.E., Fichler, C., 1999. Principal tectonic events in the evolution of the northwest European Atlantic margin. In: Fleet, A.J., Boldy, S.A.R. (Eds.), Petroleum Geology of Northwest Europe. Proceedings of the 5th Conference. Geological Society, London, 41-61.

Dumitru, T.A., 1993. A new computer-automated microscope stage system for fission-track analysis. Nuclear Tracks and Radiation Measurements 21, 557-580.

Eberl, D.D., Srodon, J., 1988. Ostwald ripening and interparticle-diffraction effects for illite crystals. American Mineralogist 73, 1335-1345.

Eig, K., Bergh, S.G., 2011. Late Cretaceous-Cenozoic fracturing in Lofoten, North Norway: Tectonic significance, fracture mechanisms and controlling factors. Tectonophysics 499, 190-205.

Faleide, J. I., Tsikalas, T., Breivik, A. J., Mjelde, R., Ritzmann, O., Engen, Ø.,

Wilson, J., Eldholm, O., 2008. Structure and evolution of the continental margin off Norway and the Barents Sea. Episodes 31, 82-91.

Faleide, J.I., Vågnes, E., Gudlaugsson, S.T., 1993. Late Mesozoic-Cenozoic evolution of the south-western Barents Sea in a regional rift-shear tectonic setting. Marine and Petroleum Geology 10, 186-214.

Frey, M., 1987. Low Temperature Metamorphism. Blackie, Glasgow.

Fuhrmann, U., Lippolt, H.J., Hess, J.C., 1987. Examination of some proposed K-Ar standards: $^{40}Ar/^{39}Ar$ analyses and conventional K-Ar data. Chemical Geology 66, 41-51.

Fürsich, F., Thompsen, E., 2005. Jurassic biota and biofacies in erratics from the Sortland area, Vesterålen, northern Norway. Geological Society of Norway Bulletin 443, 37-53.

Gabrielsen, R.H., Faleide, J.I., Pascal, C., Braathen, A., Nystuen, J.P., Etzelmuller, B., O'Donnell, S., 2010. Reply to discussion of Gabrielsen et al. (2010) by Nielsen et al.: Latest Caledonian to present tectonomorphological development of southern Norway. Marine and Petroleum Geology 27, 1290-1295.

Gabrielsen, R.H., Færseth, R.B., Jensen, L.N., Kalheim, J.E., Riis, F., 1990. Structural elements of the Norwegian continental shelf — Part I: the Barents Sea Region. Norwegian Petroleum Directorate Bulletin 6, p. 33.

Gagama, M.F.V., Eig, K., Bergh, S.G., Kløvjan, O.S., Henningsen, T., 2005. Strukturell analysa av post-kaledonske lineamenter ved Sifjorden, Vest-Senja, Troms. Abstracts and Proceedings of the Geological Society of Norway, Trondheim.

Galbraith, R.F., Laslett, G.M., 1993. Statistical models for mixed fission track ages. Nuclear Tracks 21, 459-470.

Gallagher, K., 1995. Evolving temperature histories from apatite fission-track data. Earth and Planetary Science Letters 136, 421-435.

Griffin, W. L., Taylor, P. N., Hakkinen, J. W., Heier, K. S., Iden, I. K., Krogh, E. J., Malm, O., Olsen, K. I., Ormaasen, D. E., Tveten, E., 1978. Archaean and Proterozoic crustal evolution in Lofoten-Vesteraelen, N Norway. Journal of the Geological Society of London 135, 629-647.

Haines, S.H., van der Pluijm, B.A., 2008, Clay quantification and Ar-Ar dating of synthetic and natural gouge: Application to the Miocene Sierra Mazatán detachment fault, Sonora, Mexico. Journal of Structural Geology 30, 525–538.

Hames, W. E., Andresen, A., 1996. Timing of Paleozoic orogeny and extension in the continental shelf of north-central Norway as indicated by laser $^{40}Ar/^{39}Ar$ muscovite dating. Geology 24, 1005-1008.

Hansen, J.-A. 2009. Onshore-offshore tectonic relations on the Lofoten and Vesterålen Margin - Mesozoic to early Cenozoic structural evolution and morphological implications. PhD thesis, University of Tromsø, 229 pp.

Hansen, J.-A., Bergh, S.G., 2012. Origin and reactivation of fracture systems adjacent to the Mid-Norwegian continental margin on Hamarøya, North Norway: use of digital geological mapping and morphotectonic lineament analysis. Norwegian Journal of Geology 92, 391–403.

Hansen, J.-A., Bergh, S.G., Henningsen, T., 2012. Mesozoic rifting and basin evolution on the Lofoten and Vesterålen Margin, North-Norway; time constraints and regional implications. Norwegian Journal of Geology 91, 203-228.

Hansen, J.W., Bakke, S., Fanavoll, S., 1992. Shallow drilling Nordland VI and VII 1991. Main Report, IKU report 23.

Harrison, T.M., Célérier, J., Aikman, A.B., Hermann, J., Heizler, M.T., 2009. Diffusion of ^{40}Ar in muscovite. Geochimica et Cosmochimica Acta 73, 1039-1051.

Hendriks, B.H.W., 2003. Cooling and Denudation of the Norwegian and Barents Sea Margins, Northern Scandinavia. Constrained by apatite fission track and (U-Th)/He thermochronology. PhD thesis, Vrije Universiteit Amsterdam, pp 192.

Hendriks, B., Andriessen, P., Huigen, Y., Leighton, C., Redfield, T., Murrell, G., Gallagher, K., Nielsen, B.S., 2007. A fission track data compilation for Fennoscandia. Norwegian Journal of Geology 87, 143-155.

Hendriks, B.W.H., Osmundsen, P.T., Redfield, T.F., 2010. Normal faulting and block tilting in Lofoten and Vesterålen constrained by Apatite Fission Track data. Tectonophysics 485, 154-163.

Holdsworth, R.E., 2004. Weak faults – rotten cores. Science 303, 181–182.

Hunziker, J.C., Frey, M., Clauer, N., Dallmeyer, R.D., Friedrichsen, H., Flehmig, W., Hochstrasser, K., Roggwiler, P., Schwander, H., 1986. The evolution of illite to muscovite: mineralogical and isotopic data from the Glarus Alps, Switzerland. Contributions to Mineralogy and Petrology, 92, 157–180.

Hurford, A.J., Green, P.F., 1983. The Zeta Age Calibration of Fission-Track Dating. Isotope Geoscience 1, 285 - 317.

Ketcham, R.A., 2005. Forward and inverse modelling of low-temperature thermochronometry data. Reviews in Mineralogy and Geochemistry 58, 275-314.

Ketcham, R.A., Carter, A.C., Donelick, R.A., Barbarand, J., Hurford, A.J., 2007. Improved modeling of fission-track annealing in apatite. American Mineralogist 92, 799-810.

Knutsen, S.M., Larsen, K.I., 1997. The late Mesozoic and Cenozoic evolution of the Sørvestsnaget Basin: A tectonostratigraphic mirror for regional events along the Southwestern Barents Sea margin? Marine and petroleum geology, 14, 27-54.

Lidmar-Bergström, K., Näslund, J-O., Ebert, K., Neubeck, T., Bonow, J., 2007. Cenozoic landscape development on the passive margin of northern Scandinavia. Norwegian Journal of Geology 87, 181–196.

Lidmar-Bergstrom, K., Ollier, C.D., Sulebak, J.R., 2000. Landforms and uplift history of Southern Norway. In: Chalmers-J., Cloetingh-S.A.P.L. (Eds.), Neogene uplift and tectonics around the North Atlantic. Global and Planetary Change 24 (3-4), 211-231.

Lundin, E.R., Doré, A.G. 1997. A tectonic model for the Norwegian passive margin with implications for the NE Atlantic; Early Cretaceous to break-up. Journal of the Geological Society of London 154, 545-550.

Löbens, S., Bense, F.A., Wemmer, K., Dunkl, I., Costa, C.H., Layer, P., Siegesmund, S., 2011. Exhumation and uplift of the Sierras Pampeanas: preliminary implications from K–Ar fault gouge dating and low-T thermochronology in the Sierra de Comechingones (Argentina). International Journal of Earth Sciences (Geologische Rundschau) 100, 671–694. doi 10.1007/s00531-010-0608-0.

McDougall, I., Harrison, M., 1999. Geochronology and Thermochronology by the $^{40}Ar/^{39}Ar$ method. Oxford University Press, USA.

McDougall, I., Roksandic, Z., 1974. Total fusion Ar/Ar ages using HIFAR reactor, Journal of the Geological Society of Australia 21, 81–89.

Moore, D.M., Reynolds, R.C.Jr., 1997. X-Ray Diffraction and the Identification and Analysis of Clay Minerals. Oxford University Press, USA, second ed., 378 pp.

Mosar, J., 2003. Scandinavia's North Atlantic passive margin. Journal of Geophysical

Research 108 (B8), 2360, doi:10.1029/2002JB002134

Mosar, J., Eide, E.A., Osmundsen, P.T., Sommaruga, A., Torsvik, T.H., 2002. Greenland - Norway separation: A geodynamic model for the North Atlantic. Norwegian Journal of Geology 82, 281-298.

Nielsen, S.B., Clausen, O.R., Pedersen, V.K., Leseman, J.-E., Goledowski, B., Huuse, M., Gallagher, K., Summerfield, M.A., 2010. Discussion of Gabrielsen et al. (2010): Latest Caledonian to Present tectonomorphological development of southern Norway. Marine and Petroleum Geology 27, 1285-1289.

Nielsen, S.B., Gallagher, K., Leighton, C., Balling, N., Svenningsen, L., Jacobsen, B.H., Thomsen, E., Nielsen, O.B., Heilmann-Clausen, C., Egholm, D.L., Summerfield, M.A., Clausen, O.R., Piotrowski, J.A., Thorsen, M.R., Huuse, M., Abrahamsen, N., King, C., Lykke-Andersen, H., 2009. The evolution of western Scandinavian topography: A review of Neogene uplift versus the ICE (isostasy-climate-erosion) hypothesis. Journal of Geodynamics 47, 72-95, doi:10,1016/j.jog.2008.09.001

Noble, W., 2002. MacTrack X version 1.1.1. The University of Melbourne, Australia.

Olesen, O., Torsvik, T. H., Tveten, E., Zwaan, K. B., Løseth, H., Henningsen, T., 1997. Basement structure of the continental margin in the Lofoten-Lopphavet area, northern Norway: constraints from potential field data, on-land structural mapping and palaeomagnetic data. Norsk Geologisk Tidsskrift 77, 15-30.

Olesen, O., Ebbing, J., Lundin, E., Mauring, E., Skilbrei, J. R., Torsvik, T. H., Hansen, E. K., Henningsen, T., Midbøe, P., Sand, M., 2007. An improved tectonic model for the Eocene opening of the Norwegian-Greenland Sea: Use of modern magnetic data. Marine and Petroleum Geology 24, 53-66.

Olesen, O., Lundin, E., Nordgulen, Ø., Osmundsen, P. T., Skilbrei, J. R., Smethurst, M. A., Solli, A., Bugge, T., Fichler, C., 2002. Bridging the gap between the onshore and offshore geology in Nordland, northern Norway. Norwegian Journal of Geology 82, 243-262.

Opheim, J.A., Andresen, A., 1989. Basement-cover relationships on northern Vanna, Troms, Norway. Norsk Geologisk Tidsskrift 69, 67-81.

Osmundsen, P.T., Redfield, T.F., Hendriks, B.H.W., Bergh, S.G., Hansen, J.-A., Henderson, I.H.C., Dehls, J., Lauknes, T.R., Larsen, Y., Anda, E., Davidsen, B., 2010. Fault-controlled alpine topography in Norway. Journal of the Geological Society 167, 83–98, doi: 10.1144/0016-76492009-019.

Osmundsen, P.T., Sommaruga, A., Skilbrei, J.R., Olesen, O., 2002. Deep structure of the Mid Norway rifted margin. Norwegian Journal of Geology 82, 205-224.

Pevear, D.R., 1999. Illite and hydrocarbon exploration. Proceedings of the National Academy of Sciences USA 96, 3440–3446.

Redfield, T.F., Osmundsen, P.T., 2013. The long-term topographic response of a continent adjacent to a hyperextended margin: A case study from Scandinavia. Geological Society of America Bulletin 125, 184-200.

Riis, F., 1996. Quantification of Cenozoic vertical movements of Scandinavia by correlation of morphological surfaces with offshore data. Global and Planetary Change 12, 331-357.

Schlische, R.W., Withjack, M.O., Eisenstadt, G., 2002. An experimental study of the secondary deformation produced by oblique-slip normal faulting. The American Association of Petroleum Geologists Bulletin 86, 885-906.

Solum, J.G., van der Pluijm, B.A., Peacor, D.R., 2005. Neocrystallization, fabrics and

age of clay minerals from an exposure of the Moab fault, Utah. Journal of Structural Geology 27, 1563–1576.

Steltenpohl, M.G., Hames, W.E., Andresen, A., 2004. The Silurian to Permian history of a metamorphic core complex in Lofoten, northern Scandinavian Caledonides. Tectonics 23, TC1002, doi:10.1029/2003TC001522.

Steltenpohl, M.G., Carter, B.T., Andresen, A., Zeltner, D.L., 2009. $^{40}Ar/^{39}Ar$ Thermochronology of late- and postorogenic extension in the Caledonides of North-Central Norway. The Journal of Geology 117, 399–414.

Steltenpohl, M.G., Moecher, D., Andresen, A., Ball, J., Mager, S., Hames, W.E., 2011. The Eidsfjord shear zone, Lofoten-Vesterålen, north Norway: An Early Devonian, paleoseismogenic low-angle normal fault. Journal of Structural Geology 33, 1023-1043.

Steiger, R.H., Jäger, E., 1977. Subcommission on geochronology: Convention on the use of decay constants in geo- and cosmochronology. Earth and Planetary Science Letters 36, 359-362.

Tagami, T., O'Sullivan, P.B., 2005. Fundamentals of fission-track thermochronology. Reviews in Mineralogy and Geochemistry 58, 19-47.

Talwani, M., Eldholm, O., 1977. Evolution of the Norwegian-Greenland Sea. Geological Society of America Bulletin 88, 969-999.

Tsikalas, F., Eldholm, O., Faleide, J.I., 2005. Crustal structure of the Lofoten-Vesteralen continental margin, off Norway. Tectonophysics 404, 151-174.

Tsikalas, F., Faleide, J.I., Eldholm, O., 2001. Lateral variations in tectono-magmatic style along the Lofoten-Vesterålen volcanic margin off Norway. Marine and Petroleum Geology 18, 807-832.

Tsikalas, F., Faleide, J.I., Eldholm, O., Blaich, O.A., 2012. The NE Atlantic conjugate margins. In: Roberts, D., Bally, A.W. (Eds.), Phanerozoic Passive Margins, Cratonic Basins and Global Tectonic Maps. Elsevier, 141-201.

Van der Pluijm, B.A., Hall, C.M., Vrolijk, P.J., Pevear, D.R., Covey, M.C., 2001. The dating of shallow faults in the Earth`s crust. Nature 412, 172–175.

Viola, G., Venvik Ganerød, G., Wahlgren, C.-H., 2009. Unravelling 1.5 Gyr of brittle deformation history in the Laxemar-Simpevarp area, SE Sweden: a contribution to the Swedish site investigation study for the disposal of highly radioactive nuclear waste. Tectonics 28, TC5007.

Viola, G., Zwingmann, H., Mattila, J., Käpyaho, A., 2013. K-Ar illite age constraints on the Proterozoic formation and reactivation history of a brittle fault in Fennoscandia. Terra Nova 25, 236-244, doi:10.1111/ter.12031.

Waqas, A., 2012. Structural analysis of the Troms-Finnmark fault complex, SW Barents Sea. MSc thesis, University of Oslo, pp. 143.

Wemmer, K., 1991. K/Ar-Altersdatierungsmöglichkeiten für retrograde Deformationsprozesse im spröden und duktilen Bereich - Beispiele aus der KTB-Vorbohrung (Oberpfalz) und dem Bereich der Insubrischen Linie (N-Italien). - Göttinger Arbeiten Geologie und Paläontologie 51, 1-61.

Wilson, R.W., McCaffrey, K.J.W., Holdsworth, R.E., Imber, J., Jones, R.R., Welbon, A.I.F., Roberts, D., 2006. Complex fault patterns, transtension and structural segmentation of the Lofoten Ridge, Norwegian margin; using digital mapping to link onshore and offshore geology. Tectonics 25, TC4018, doi:10.1029/2005TC001895.

Ziegler, P.A., 1989. Evolution of the North Atlantic; an overview. AAPG Memoir 46, 111-129.

Zwingmann, H., Han, R., Ree, J.-H., 2011. Cretaceous reactivation of the Deokpori Thrust, Taebaeksan Basin, South Korea, constrained by K-Ar dating of clayey fault gouge. Tectonics 30, TC5015 , doi:10.1029/2010TC002829.

Zwingmann, H., Mancktelow, N., 2004. Timing of Alpine fault gouges. Earth and Planetary Science Letters 223, 415–425.

Zwingmann, H., Mancktelow, N., Antognini, M., Lucchini, R., 2010. Dating of shallow faults: New constraints from the AlpTransit tunnel site (Switzerland). Geology 38, 487-490.

Zwaan, K.B., 1995. Geology of the West Troms Basement Complex, northern Senja, with emphasis on the Senja Shear belt: a preliminary account. Norges geologiske undersøkelse Bulletin 427, 33-36.

Figure Captions

Figure 1. Simplified structural geological map of Norway and the Norwegian continental margin with location of the study area (modified after Mosar et al. (2002) and Hansen (2011)). Abbreviations: BSFC: Bothnian-Senja Fault Complex; HFFZ: Hadselfjorden Fault Zone; VVFC: Vestfjorden-Vanna Fault Complex; WLBFZ: West Lofoten Border Fault Zone.

Figure 2. Simplified geological map of the study area with sample locations of the fault gouges. Faults are compiled from Mosar et al. (2002) and Hansen (2011). Abbreviations: BSFC: Bothnian-Senja Fault Complex; HFFZ: Hadselfjorden Fault Zone; SEF: Stongelandseidet Fault; VF: Vannareid Fault VVFC: Vestfjorden-Vanna Fault Complex; WLBFZ: West Lofoten Border Fault Zone. Sample locations: 1. Laksvatn; 2. Vanna; 3. Sifjord; 4. Andøya; 5. Rødsand; 6. Ryggedalsvatn; Straumsnes; 8. Instøya; 9. Myre.

Figure 3. Photos of the sampled faults, yellow circles indicate sampling location: a. Laksvatn; b. Vanna; c. Andøya, solid yellow line indicates the location of the sampled fault gouge, dashed lines outline slickensides; d. Rødsand; e. Ryggedalsvatn; f. Instøya; Insets show equal area projections with main fracture orientations plotted as black great circles, minor fractures as grey great circles, main lineations as black dots and minor lineations as open grey dots.

Figure 4. Photos of the sampled faults. A. Sifjord; b. Straumsnes north (Straumsnes 1); c. Straumsnes south (Straumsnes 2). Insets show equal area projections with main fracture orientations plotted as black great circles, minor fractures as grey great circles, main lineations as black dots and minor lineations as open grey dots.

Figure 5. Rose diagram of the 10 fault orientations.

Figure 6. K-Ar illite results with simplified geological history as summarised in section 2. AFT: AFT ages reported in section 4.4; AFT LVA: AFT ages reported by Hendriks et al. (2010).

Figure 7. Polar plot of K-Ar illite ages versus fault orientations.

Figure 8. A. SEM image of Laksvatn fault gouge sample < 2mm showing platy and fibrous illite particles (I), illite confirmed by EDS. B. TEM image of Vanna fault gouge < 2mm showing platy and fibrous illite morphology (I).

Figure 9. Simplified geological map with AFT results (AFT ages in Ma). Legend as in Fig. 1 and 2; location indicated in Fig. 1. Abbreviations: SB: Store Blåmann; SEF: Stongelandseidet Fault; TT: Tromsdalstinden; VF: Vannareid Fault; VVFC: Vestfjorden-Vanna Fault Complex.

Figure 10. AFT ages versus D_{par} values.

Figure 11. AFT ages across the northerly WNW-ESE transect (A-A' in Fig. 9). Filled circles are the AFT ages; open triangles D_{par} values. WTBC: West Troms Basement Complex.

Figure 12. Vertical AFT age profile of the mountain Store Blåmann (Fig. 9).

Figure 13. AFT thermal history models and track length distributions. The models were run until 100 good fit paths were found. Pink paths are good fit, green paths are acceptable fit. The PAZ is the temperature range between the dashed black lines at 120˚C and 60˚C; the models are more significant within this region than outside. Blue boxes indicate the modelling constraints.

Table Captions

Table 1. K-Ar illite results.

Table 2. XRD results of the fault gouge samples.

Table 3. AFT counting results. A personal zeta factor of 261.5 ± 6.1 was used for counting. MTL: mean track length.

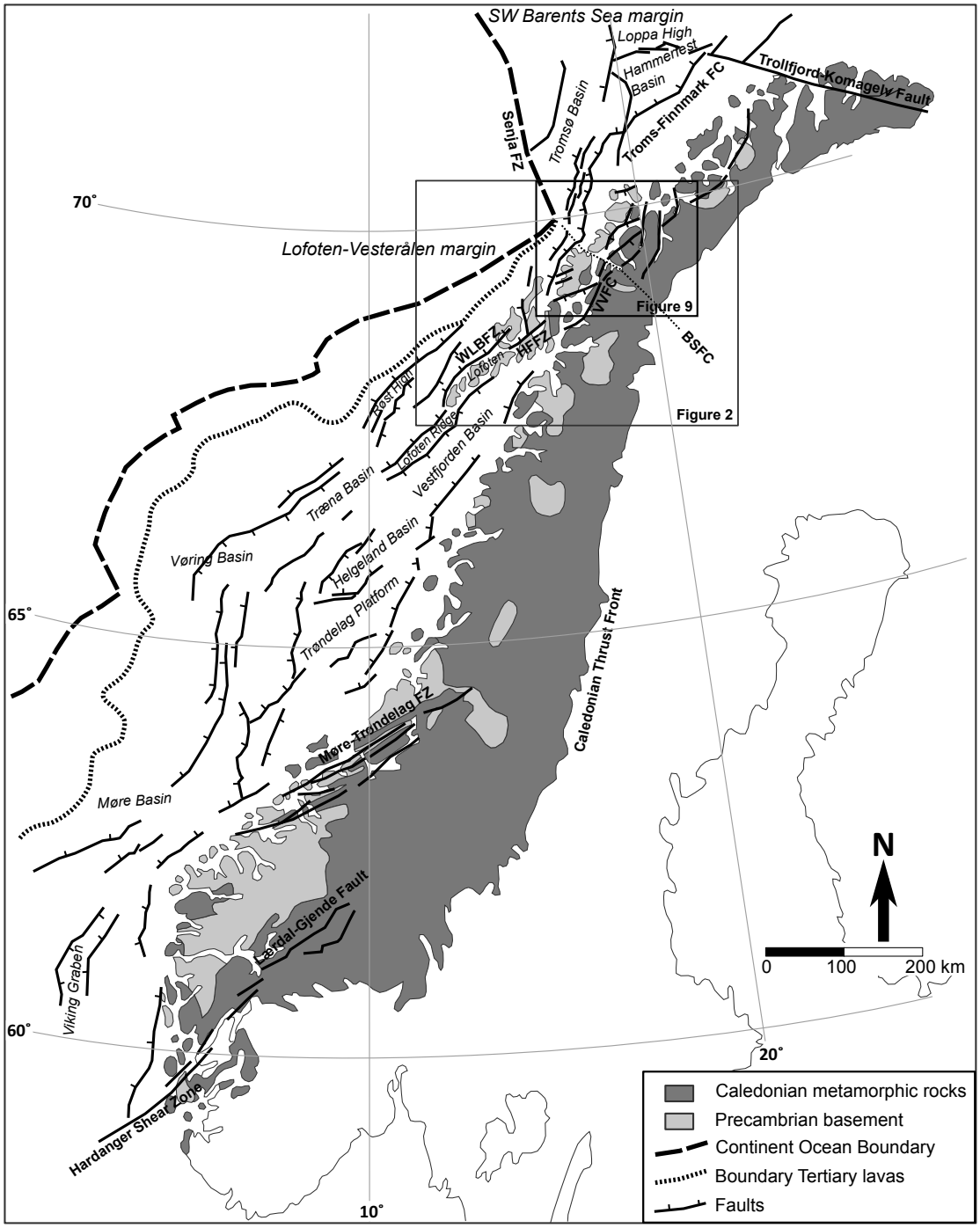
SW Barents Sea margin
Loppa High
Hammerfest Basin
Troms-Finnmark FC
Trollfjord-Komagelv Fault
Senja FZ
Tromsø Basin
70°
Lofoten-Vesterålen margin
Figure 9
VVFC
BSFC
WLBFZ
HFFZ
Lofoten
Røst High
Lofoten Ridge
Vestfjorden Basin
Figure 2
Træna Basin
Vøring Basin
Helgeland Basin
Trøndelag Platform
65°
Caledonian Thrust Front
Møre-Trøndelag FZ
Møre Basin
Jæren-Gjende Fault
Viking Graben
60°
Hardanger Shear Zone
10°
20°
N
0
100
200 km
Caledonian metamorphic rocks
Precambrian basement
Continent Ocean Boundary
Boundary Tertiary lavas
Faults

Figure 1.

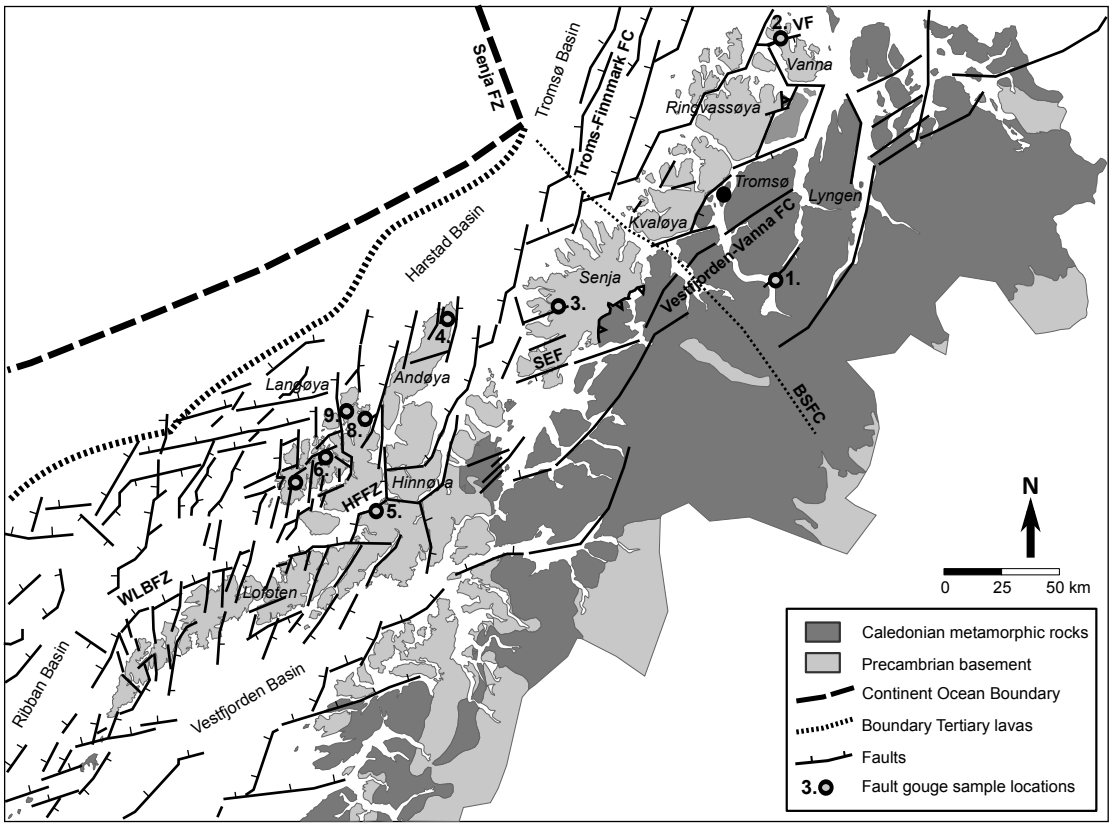
Senja FZ
Tromsø Basin
Troms-Finnmark FC
2. VF
Vanna
Ringvassøya
Tromsø
Lyngen
Kvaløya
Harstad Basin
Senja
3.
1.
Vestfjorden-Vanna FC
4.
SEF
Langøya
Andøya
9.
8.
6.
7.
Hinnøya
HFFZ
5.
BSFC
N
0 25 50 km
WLBFZ
Lofoten
Ribban Basin
Vestfjorden Basin
Caledonian metamorphic rocks
Precambrian basement
Continent Ocean Boundary
Boundary Tertiary lavas
Faults
3. Fault gouge sample locations

Figure 2.

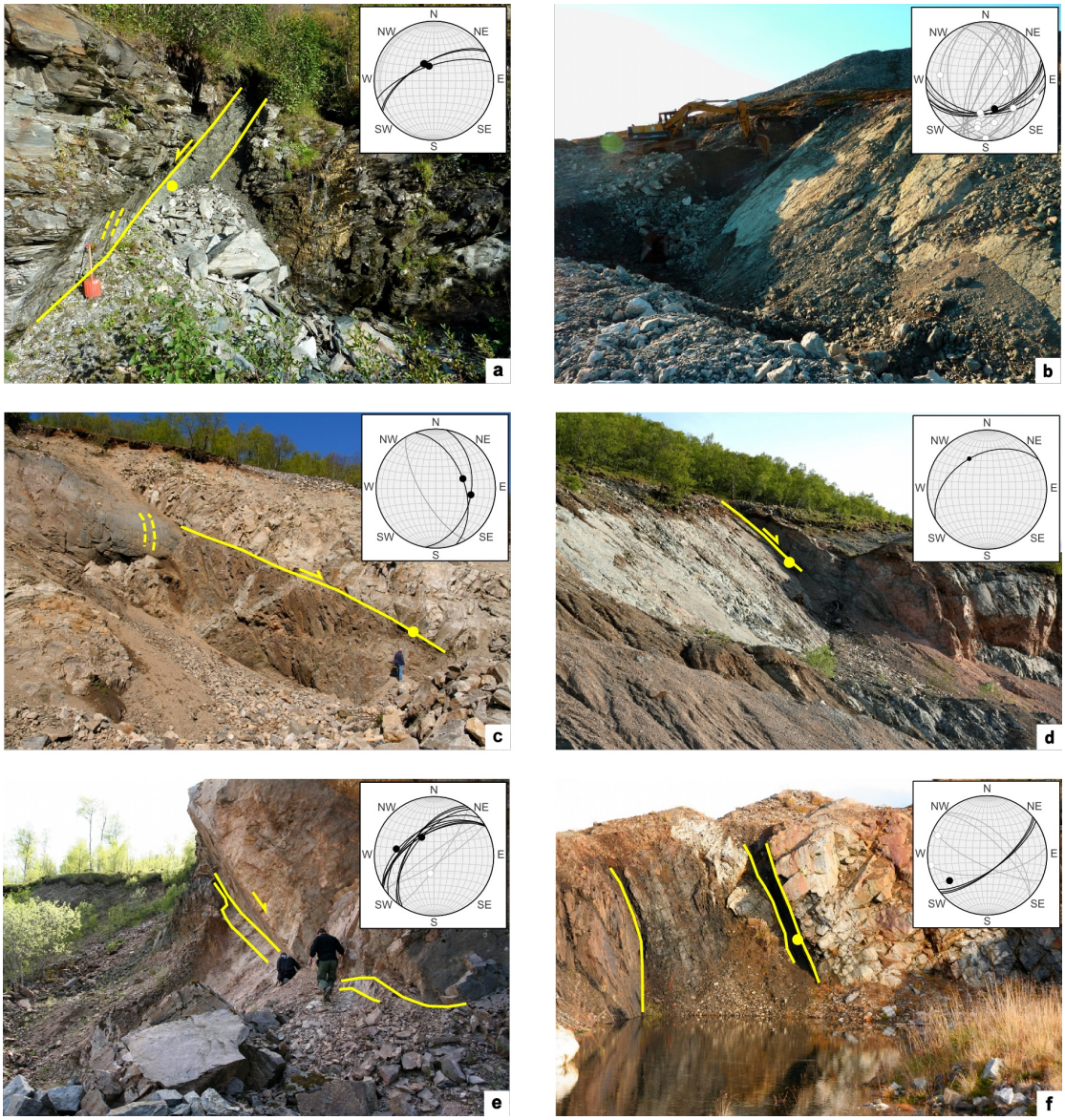

Figure 3.

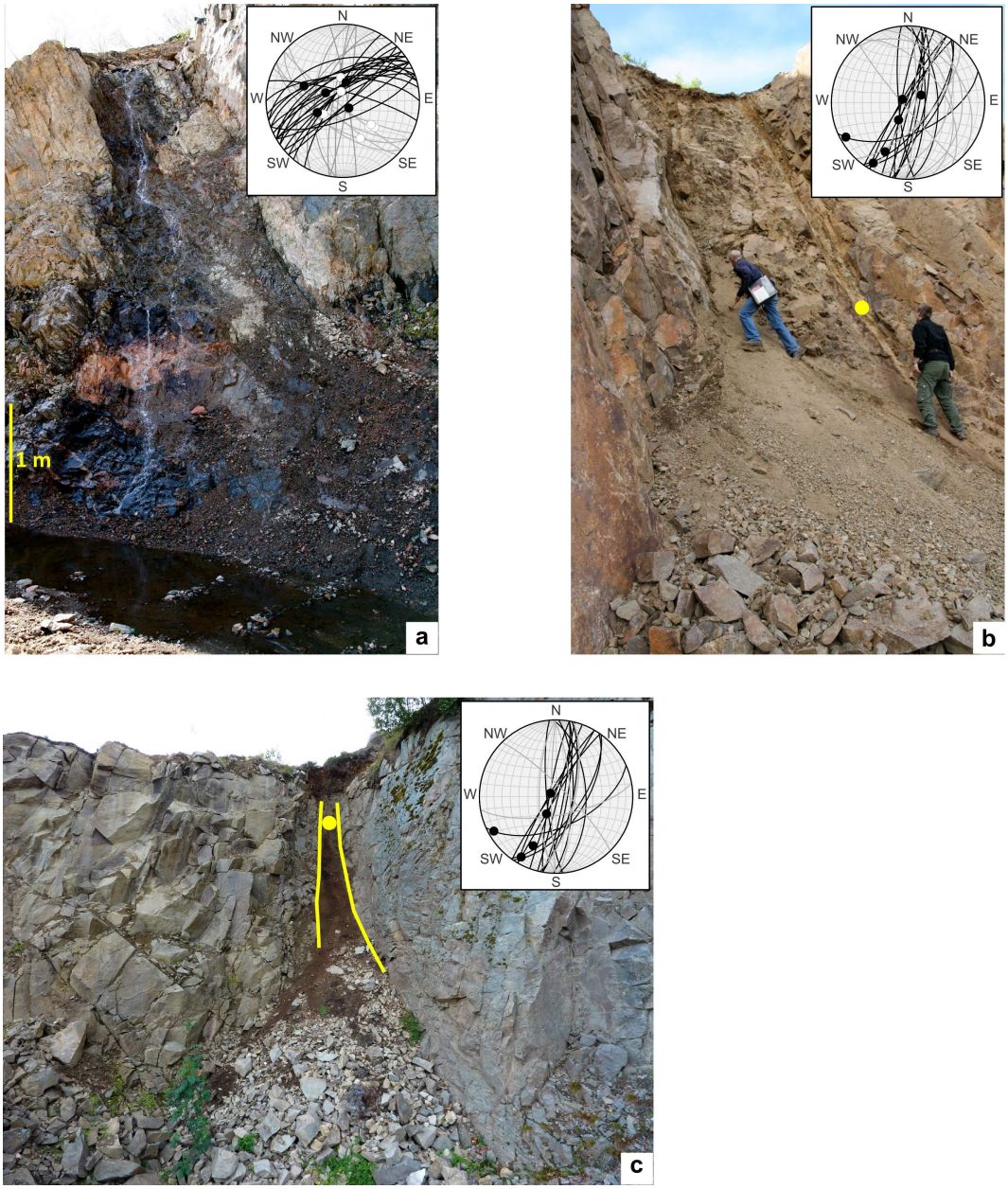

Figure 4.

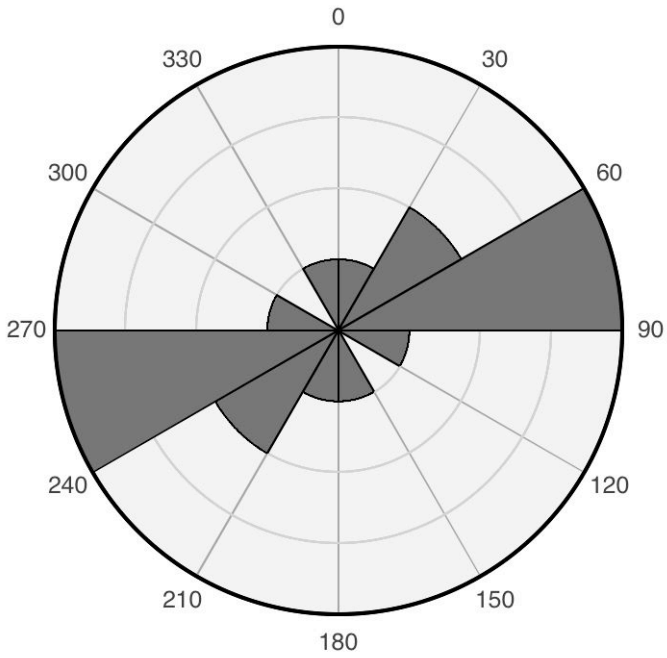

Figure 5.

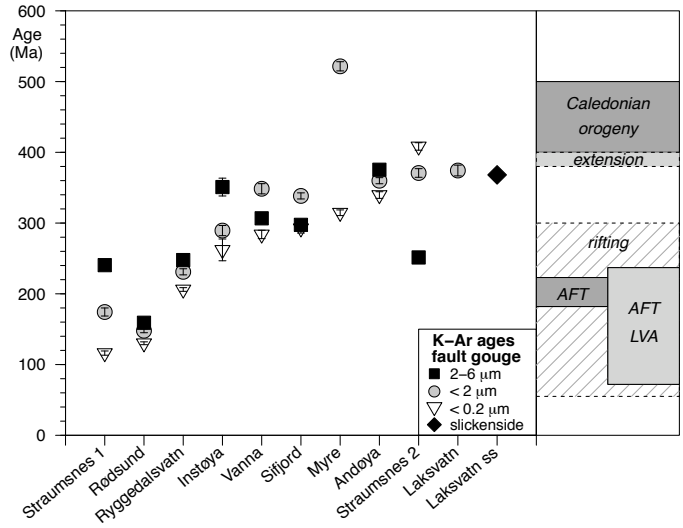
600
Age
(Ma)
500
400
300
200
100
0
Caledonian
orogeny
extension
rifting
AFT
AFT
LVA
K–Ar ages
fault gouge
2–6 μm
< 2 μm
< 0.2 μm
slickenside
Straumsnes 1
Rødsund
Ryggedalsvatn
Instøya
Vanna
Sifjord
Myre
Andøya
Straumsnes 2
Laksvatn
Laksvatn ss

Figure 6.

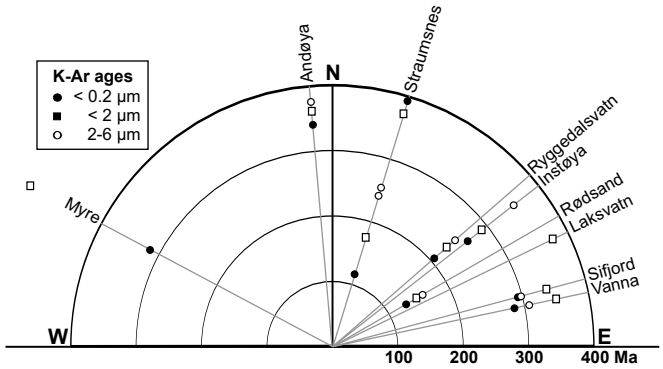
K-Ar ages
< 0.2 µm
< 2 µm
2-6 µm
N
W
E
Andøya
Straumsnes
Ryggedalsvatn
Instøya
Rødsand
Laksvatn
Sifjord
Vanna
Myre
100
200
300
400 Ma

Figure 7.

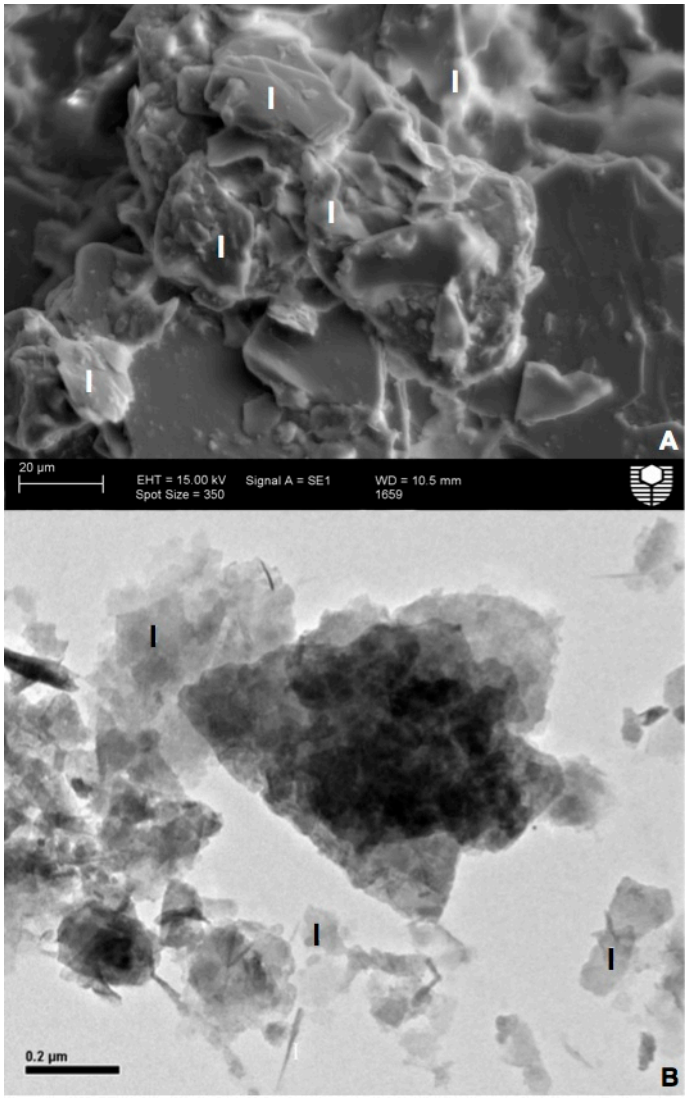
A
20 µm
EHT = 15.00 kV
Spot Size = 350
Signal A = SE1
WD = 10.5 mm
1659
0.2 µm
B

Figure 8.

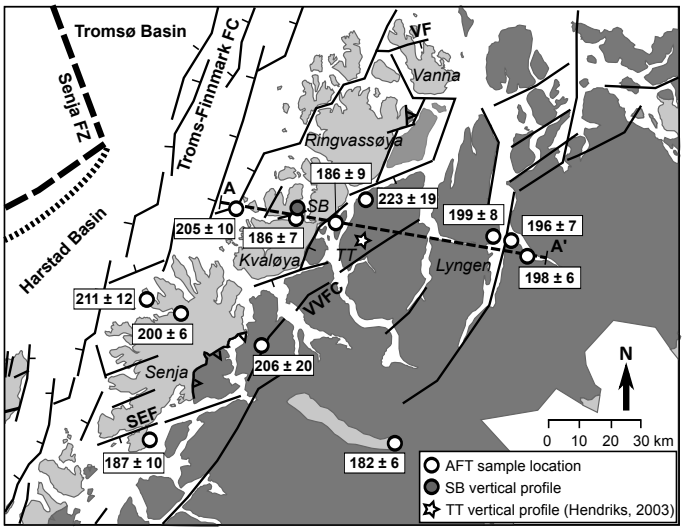
Tromsø Basin
Senja FZ
Troms-Finnmark FC
Harstad Basin
VF
Vanna
Ringvassøya
186 ± 9
223 ± 19
199 ± 8
196 ± 7
198 ± 6
A
A'
SB
TT
205 ± 10
186 ± 7
Kvaløya
Lyngen
211 ± 12
200 ± 6
VVFC
206 ± 20
Senja
SEF
187 ± 10
182 ± 6
N
0 10 20 30 km
AFT sample location
SB vertical profile
TT vertical profile (Hendriks, 2003)

Figure 9.

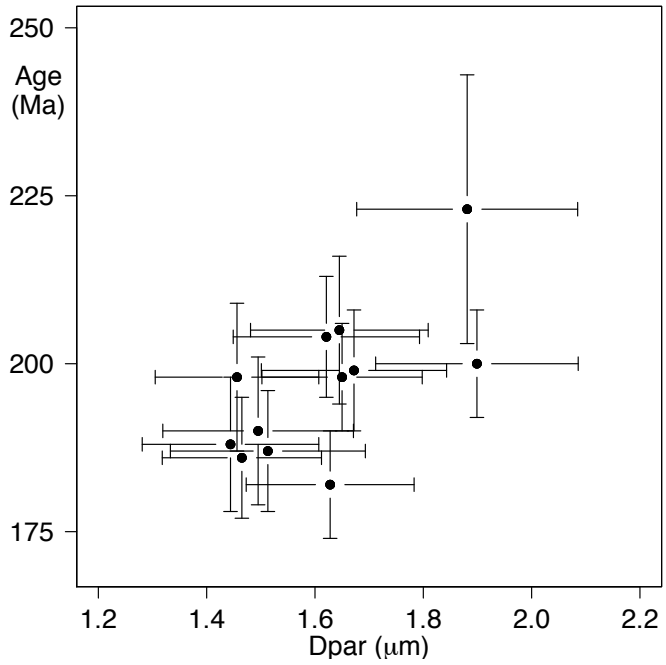

Figure 10.

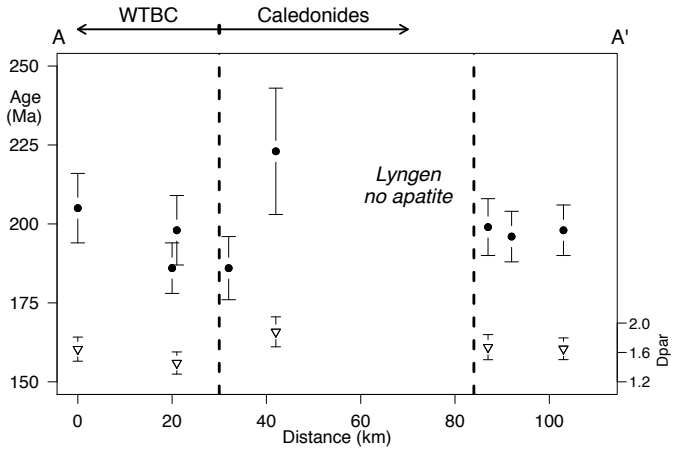
WTBC
Caledonides
A
A'
250
Age
(Ma)
225
200
175
150
Lyngen
no apatite
2.0
1.6
1.2
Dpar
0
20
40
60
80
100
Distance (km)

Figure 11.

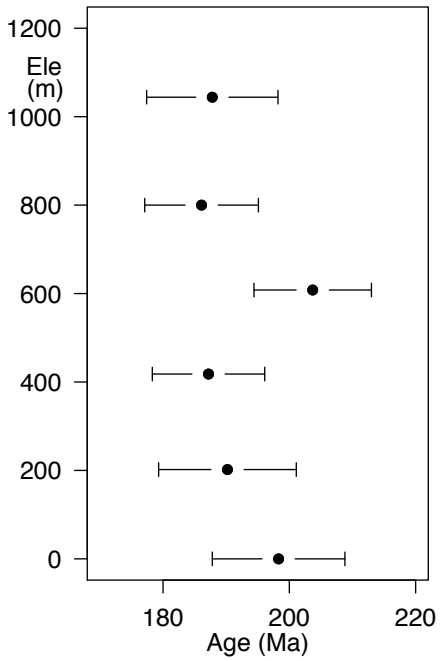

Figure 12.

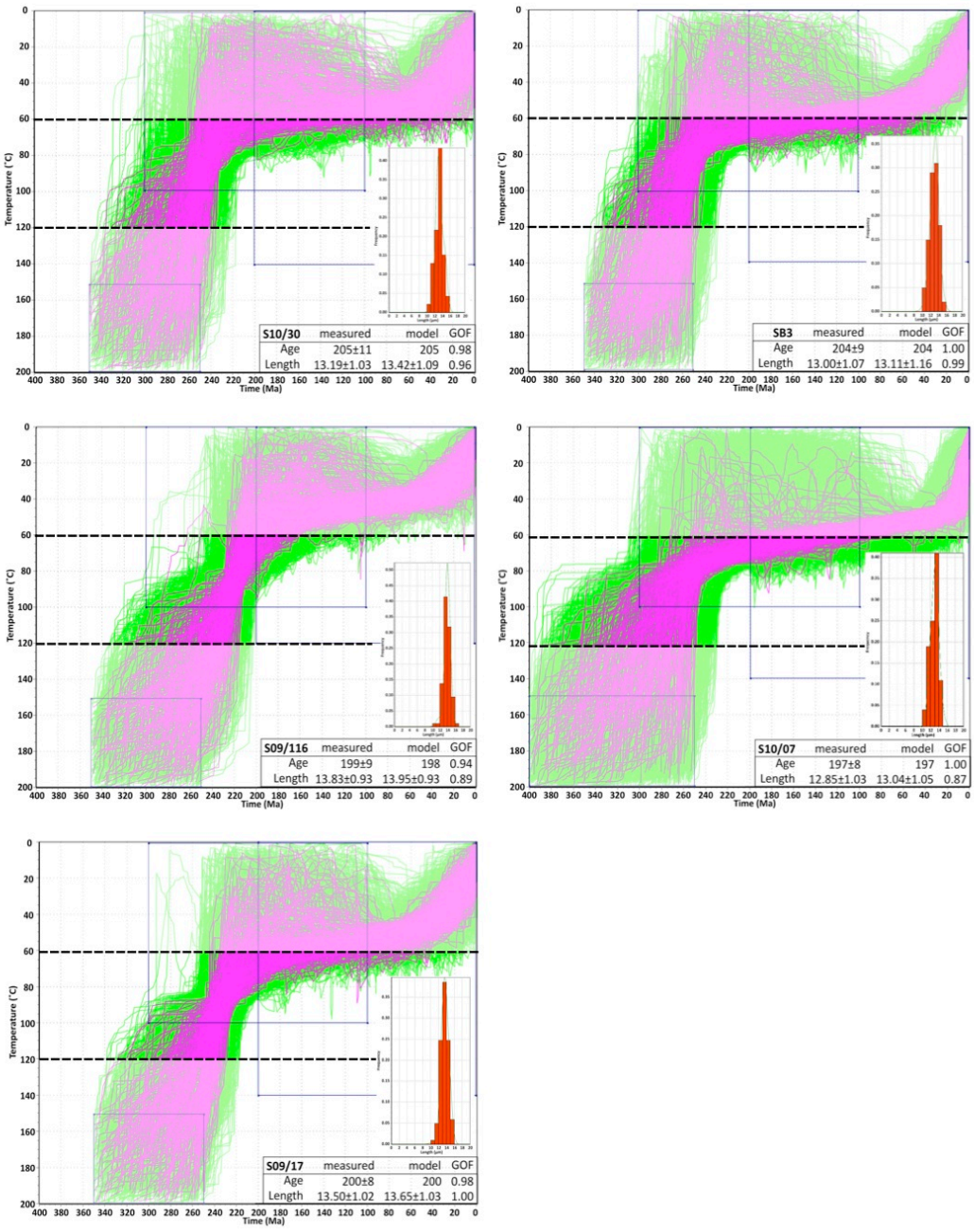
Temperature (°C)
Time (Ma)
S10/30 measured model GOF
Age 205±11 205 0.98
Length 13.19±1.03 13.42±1.09 0.96
SB3 measured model GOF
Age 204±9 204 1.00
Length 13.00±1.07 13.11±1.16 0.99
S09/116 measured model GOF
Age 199±9 198 0.94
Length 13.83±0.93 13.95±0.93 0.89
S10/07 measured model GOF
Age 197±8 197 1.00
Length 12.85±1.03 13.04±1.05 0.87
S09/17 measured model GOF
Age 200±8 200 0.98
Length 13.50±1.02 13.65±1.03 1.00

Figure 13.